a NATO Research Centre
un Centre de Recherche de l'OTAN

PARTNERING FOR MARITIME INNOVATION

Technical Report NURC-FR-2011-001

The relation between the waveguide invariant, multipath impulse response, and ray cycles

Chris Harrison

February 2011

About NURC

Our vision

- To conduct maritime research and develop products in support of NATO's maritime operational and transformational requirements.
- To be the first port of call for NATO's maritime research needs through our own expertise, particularly in the undersea domain, and that of our many partners in research and technology.

One of three research and technology organisations in NATO, NURC conducts maritime research in support of NATO's operational and transformation requirements. Reporting to the Supreme Allied Commander, Transformation and under the guidance of the NATO Conference of National Armaments Directors and the NATO Military Committee, our focus is on the undersea domain and on solutions to maritime security problems.

The Scientific Committee of National Representatives, membership of which is open to all NATO nations, provides scientific guidance to NURC and the Supreme Allied Commander Transformation.

NURC is funded through NATO common funds and respond explicitly to NATO's common requirements. Our plans and operations are extensively and regularly reviewed by outside bodies including peer review of the science and technology, independent national expert oversight, review of proposed deliverables by military user authorities, and independent business process certification.

The relation between the waveguide invariant, multipath impulse response, and ray cycles

Chris Harrison

This document, which describes work performed under the Project Cooperative ASW of the NURC Scientific Programme of Work, has been approved by the Director.

Intentionally blank page

The relation between the waveguide invariant, multipath impulse response, and ray cycles

Chris Harrison

Executive Summary: Underwater sound propagation, being a wave phenomenon, exhibits interference effects, as is well known. With broad band sonars it is often possible to see this interference across a wide band of frequencies as source and receiver separate in range. The resulting pattern viewed in frequency-range space exhibits interference fringes, often referred to as "striations", which appear as streaks or lines which may converge or diverge in frequency as range increases. This phenomenon, though at first sight just a curiosity, depends mainly on the sound speed structure and the depths of the source and receiver. For this reason it has been of great interest in separating target echoes out from reverberation. The frequency spectrum of reverberation as a function of travel time can also be thought of as a plot of frequency vs. range, so one would expect it to show striations directly. If so, the striations provide the potential to separate targets from reverberation and to estimate their depth.

The "waveguide invariant", β, that controls the striations, is usually thought of as a modal phenomenon. This report shows that striations can be explained simply through the variation of the eigenray arrival times with range, in short, the variation of the multipath impulse response. It is possible to calculate β for a number of sound speed profiles analytically and to see what β depends on, why it switches from one value to another, how it depends on source-receiver depth, and so on. The analytical findings are confirmed by calculating striation patterns numerically starting from eigenray travel times in various stratified environments. Most importantly the approach throws some light on what can be deduced from β alone and the likelihood and utility of striations in reverberation.

Intentionally blank page

The relation between the waveguide invariant, multipath impulse response, and ray cycles

Chris Harrison

Abstract: The waveguide invariant, β, that manifests itself as interference fringes or "striations" in a plot of frequency vs source-receiver separation, is usually thought of as a modal phenomenon. This report shows that striations can be explained simply through the variation of the eigenray arrival times with range, in short, the variation of the multipath impulse response. It is possible to calculate β for a number of sound speed profiles analytically and to see what β depends on, why it switches from one value to another, how it depends on source-receiver depth, how it depends on variable bathymetry, and how smooth the sound speed profile needs to be for clear fringes. The analytical findings are confirmed by calculating striation patterns numerically starting from eigenray travel times in various stratified environments. Most importantly the approach throws some light on what can be deduced from β alone and the likelihood and utility of striations in reverberation.

Keywords: Waveguide invariant, interference fringe, striation, sound speed profile, closed-form solution, analytical solution, time domain.

Contents

1 Introduction

The behaviour of propagation interference fringes or “striations” as sound source and receiver are separated can be quantified through a “waveguide invariant” called β (Chuprov, 1982; Brekhovskikh and Lysanov, 1990; D’Spain and Kuperman, 1999; Brown, Beron-Vera, Rypina, Udovydchenkov, 2005). A special case of these striations is the hyperbolic Lloyd mirror fringes that have been used in passive ranging, allowing determination of closest point of approach and ratio of range to source depth (Hudson, 1983; Turgut, Orr, and Rouseff, 2010). More general range localization is discussed by Cockrell and Schmidt (2010) and Søstrand (2005). In recent years β has been considered as part of the toolset in geoacoustic inversion (Heaney, 2004) and has been applied to the detection of targets and reverberatrion estimation (Goldhahn, Hickman and Krolik, 2008) and active sonar (Quijano, Zurk, and Rouseff, 2008). It has also been tied into such topics as time reversal focusing (Kim, Kuperman, Hodgkiss, Song, Edelman, and Akal, 2003), fluctuation statistics (Rouseff, 2002), and beam processing (Yang, 2003).

Most attempts at understanding the patterns have been through the normal modes of the waveguide. A complementary interpretation is that the behaviour of the fringes is determined by the behaviour of the impulse response as the receiver is moved, and this is the approach taken in this paper. Since it is possible to calculate the delay times of eigenrays numerically and in some cases analytically it is then possible, by writing out their Fourier transform, to see how the fringes will behave. Because thinking in terms of the impulse response is fairly intuitive this approach adds some insight to the more conventional modal method, and in some cases even enables qualitative solution without detailed computation.

In the high frequency limit the multipath impulse response consists of many positive and negative impulses that correspond to the many eigenrays. The introduction of boundary reflections, caustics, rough surfaces, low frequencies certainly alters the detailed shape of these impulses, and refractioon may alter the sequence but nevertheless the fringe pattern at a given range is the Fourier transform of this impulse response. As the range between source and receiver changes the time ordering of the individual impulses generally does not change but their separation does. If the time separations widen then the fringe separation in frequency reduces in proportion, and vice versa.

2 Demonstration

First we give a simple numerical demonstration of this by numerically calculating eigenray arrival times and rough amplitudes (including signs) by using a very crude representation of reflection loss which automatically makes the sequence of impulses tail off, but no allowance for caustics, and so on. However, as we will see later, this envelope shape is not important. The fringe pattern is just the modulus-square of the Fourier transform of this impulse response.

2.1 Isovelocity case

Figure 1 is a plot of frequency vs. source/receiver separation for isovelocity water with crudely modelled boundaries and mid-depth source and receiver. In this case the shape of the fringes is well known and they radiate from zero range. In fact generally the dependence of the interference fringes on range can be quantified as the slope of d(logω) / d(log r), i.e. the quantity "β"

$$\beta = \frac{d\omega / dr}{\omega / r} \tag{1}$$

The fringes here are demonstrably linear with r, and this results in $\beta = 1$.

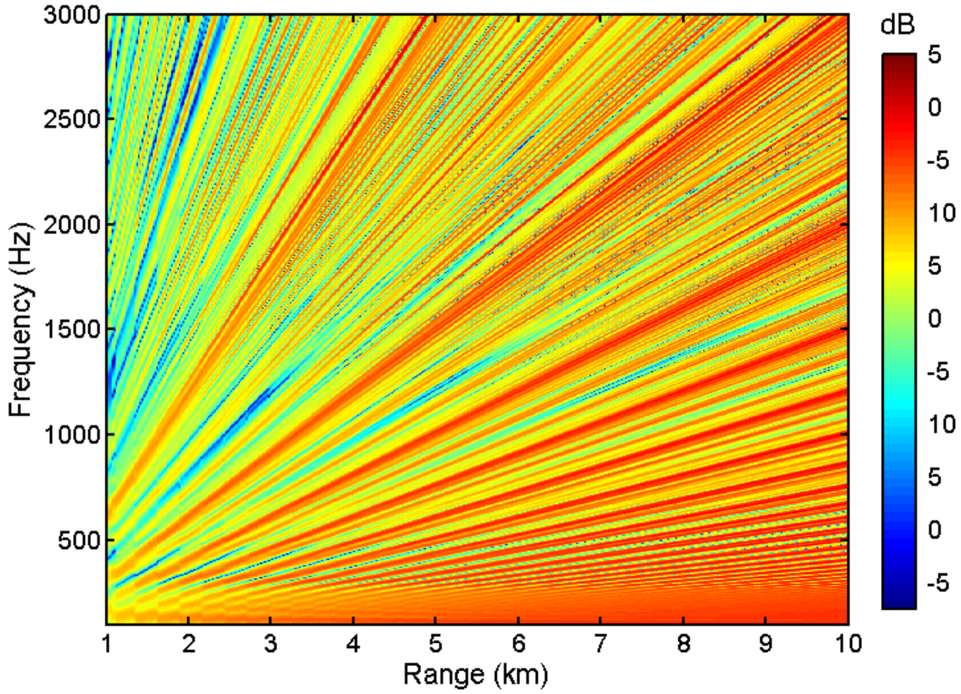

Figure 1: The spectrum of propagation vs. range derived from isovelocity travel times. Striations obeying $\omega \propto r$ are clear.

2.2 Uniform sound speed gradient case

It is straightforward for an arbitrary set of elevation angles and a general sound speed profile to calculate full ray cycle distance and cycle time and the partial equivalents for the source and receiver depths. Then, by interpolation, given each range, one can calculate the travel times of all eigenrays that are able to reach the receiver. The resulting frequency-range plot for a uniform sound speed gradient (1500m/s down to 1470m/s at the seabed) is shown in Fig. 2. Source and receiver depths (90, 91m) in 100m water depth were chosen to ensure a wide range of angles. The behaviour is again well known, but now the fringes curve the other way and $\omega \propto r^{-3}$ so $\beta = -3$.

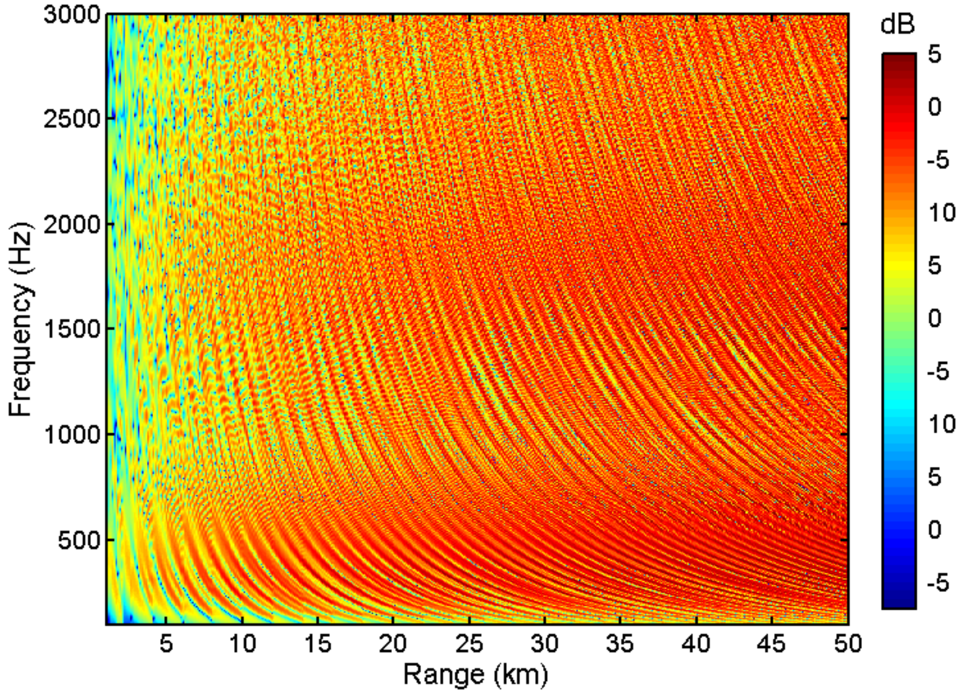

Figure 2: The spectrum of propagation vs. range derived from eigenray travel times when sound speed has a uniform gradient. Striations obeying $\omega \propto r^{-3}$ are clear.

3 Analysis

The basic behaviour of these fringes and their beta value can be calculated analytically in several cases of interest.

3.1 Isovelocity

By the method of images it is straightforward to show that the eigenrays arriving at horizontal range *r* occur at angles θ_n given by

$$\tan\theta_{n,\mu,\nu} = (2nH + \mu z_s + \nu z_r)/r \tag{2}$$

where *n* is an integer, *H* is water depth, $z_{s,r}$ are source and receiver depth, and μ, ν both take values +1 and –1. Travel time is simply

$$t_{n,\mu,\nu} = r\sec\theta_{n,\mu,\nu}/c \tag{3}$$

and the delay after the first return is

$$\tau_{n,\mu,\nu} = \frac{r}{c}(\sec\theta_{n,\mu,\nu} - 1) \tag{4}$$

In the small angle approximation this combined with Eq. (2) becomes

$$\tau_{n,\mu,\nu} = (2nH + \mu z_s + \nu z_r)^2/(2rc) \tag{5}$$

In the eigenray approximation the impulse response consists of a weighted sequence of delta functions at the delays defined by $\tau_{n,\mu,\nu}$, and consequently the Fourier transform of the impulse response $F(\omega, r)$, whose modulus square is the fringe pattern, is

$$\begin{aligned} F(\omega,r) &= \int \sum_{\mu,\nu} \sum_n a_n\, \delta(\tau - \tau_{n,\mu,\nu}) \exp(i\omega\tau)\, d\tau \\ &= \sum_{\mu,\nu} \sum_n a_n \exp(i\omega\tau_{n,\mu,\nu}) \end{aligned} \tag{6}$$

The summation over μ,ν means that for each value of *n* in Eq. (2) there are four combinations of μ and ν over which we should also sum. These four terms result in two positive and two negative signs multiplied by almost identical values of the weighting a_n. Thus we can think of Eq. (6) as four separate summations over *n* in each of which a_n is a positive slowly varying function of *n* – in effect an envelope.

$$F(\omega,r) = -\sum_n a_n \exp(i\omega\tau_{n,+1,+1}) - \sum_n a_n \exp(i\omega\tau_{n,-1,-1}) + \sum_n a_n \exp(i\omega\tau_{n,+1,-1}) + \sum_n a_n \exp(i\omega\tau_{n,-1,+1}) \qquad (7)$$

Substituting Eq. (5) in Eq. (6) for τ_n, and for the moment ignoring the slow variation of a_n we find

$$\begin{aligned} F(\omega,r) &= -\sum_n a_n \exp\big(i(\omega/r)(2nH + z_s + z_r)^2/(2c)\big) \\ &\quad -\sum_n a_n \exp\big(i(\omega/r)(2nH - z_s - z_r)^2/(2c)\big) \\ &\quad +\sum_n a_n \exp\big(i(\omega/r)(2nH + z_s - z_r)^2/(2c)\big) \\ &\quad +\sum_n a_n \exp\big(i(\omega/r)(2nH - z_s + z_r)^2/(2c)\big) \\ &= G(\omega/r) \end{aligned} \qquad (8)$$

Thus the complex Fourier transform F is explicitly a function of ω/r, so no matter what its functional form is it has only one shape as ω and r vary. At any given r there will be a fringe pattern in ω, but moving to a different value of r we find the *same* pattern but stretched in ω in proportion to the increase in r. This automatically constructs a fringe pattern where the modulation takes a constant value along lines where $\omega \propto r$. In other words the condition for a fringe is that

$$\frac{\omega}{r} = A = \text{constant} \qquad (9)$$

Taking logs and differentiating, we find this obeys Eq. (1) with $\beta = 1$, exactly as was found in Fig. 1.

The weights a_n can be written out in terms of reflection coefficients, etc., although since their variation is always much slower than that of the impulses their influence must be small and it does not alter the above argument. It was shown by Harrison and Nielsen (2007) that, for instance, in isovelocity water the one-way multipath pulse envelope decays approximately exponentially with time.

3.2 General refracting environments

We now extend these ideas to a general refracting environment by attempting to write the Fourier transform in a form that again demonstrates explicitly the functional dependence on ω and r.

For a general stratified environment the eigenrays for horizontal separation r obey

$$r = nr_c(\theta_{n,\mu,\nu}) + \mu r_s(\theta_{n,\mu,\nu}) + \nu r_r(\theta_{n,\mu,\nu}) \qquad (10)$$

where r_c is the cycle distance (double the result of integrating from the top ray turning point to the bottom ray turning point) and r_s , r_r are the partial cycle distances from the top turning point down to the source and receiver depths respectively. Explicit formulas will be given later. The corresponding eigenray travel times are

$$t_{n,\mu,\nu}(r) = nt_c(\theta_{n,\mu,\nu}) + \mu t_s(\theta_{n,\mu,\nu}) + \nu t_r(\theta_{n,\mu,\nu}) \tag{11}$$

where the t_c , t_s , t_r are the full cycle and partial cycle travel times corresponding to r_c , r_s , r_r .

Equation (7) is true in general but with the behaviour of $\tau_{n,\mu,\nu}$ depending on sound speed profile. So we expect similar relations to Eq. (8) but with the resultant G being a function of the product of ω with some different function of r. As it stands these fringes are in the complex quantity F. Alternatively what is often observed is the modulus square of F, so the cross terms in $|F|^2$ may be important, and these depend on ($t_{n,\mu,\nu} - t_{m,\mu,\nu}$). It transpires that the value of β is very slightly different in the two cases (see Sect. A3 of Appendix A), and we estimate them both below. In the first case we investigate the delay time $\tau_{n,\mu,\nu}$ after some range-dependent datum, and we arbitrarily choose range r divided by the minimum sound speed in the profile c_L.

3.3 Condition for a fringe in absolute phase

We need to investigate the delay time $\tau_{n,\mu,\nu}$ after some range-dependent datum, and we arbitrarily choose range r divided by the minimum sound speed in the profile c_L. So $\tau_{n,\mu,\nu}$ can be expressed as

$$\begin{aligned}\tau_{n,\mu,\nu}(r) &= nt_c + \mu t_s + \nu t_r - r/c_L \\ &= n\left(t_c - \frac{r_c}{c_L}\right) + \mu(t_s - \frac{r_s}{c_L}) + \nu(t_r - \frac{r_r}{c_L}) \\ &= r\left(\frac{t_c}{r_c} - \frac{1}{c_L}\right) + \mu r_s\left(\frac{t_s}{r_s} - \frac{t_c}{r_c}\right) + \nu r_r\left(\frac{t_r}{r_r} - \frac{t_c}{r_c}\right)\end{aligned} \tag{12}$$

As in the isovelocity case the eigenray impulses still come in groups of four, two positive and two negative, and the separations within a group ($\tau_{n,\pm1,\pm1} - \tau_{n,\pm1,\pm1}$) are always smaller than the group separation ($\tau_{n+1,\mu,\nu} - \tau_{n,\mu,\nu}$) (see Appendix A, Sect. A2). Therefore fringes due to the group separation will be more closely spaced in frequency and more visible than those due to the separation of the members of the group, so we concentrate on group separation. We define the group centre as the point $\tau_{n,0,0}$ which is almost identical to the mean of the group.

$$\tau_{n,0,0}(r) = r\left(\frac{t_c(\theta_{n,0,0})}{r_c(\theta_{n,0,0})} - \frac{1}{c_L}\right) \tag{13}$$

The equivalent of Eq. (7) for the groups is

$$\hat{F}(\omega,r)=\sum_n a_n \exp(i\omega\tau_{n,0,0}) \tag{14}$$

As argued earlier (after Eq.(8)), to see fringes it must be possible to write $\tau_{n,0,0}$ as the product of a function of range only and a function of all the other parameters (e.g. n, H, z_s etc.). In other words in the exponent of Eq. (14) the range dependence must be separable. This ensures that in going from one range to the next the Fourier transform $\hat{F}$ may shrink or stretch slightly but always retains its shape. That property forms the striation pattern. Without that property there is no fringe pattern since $\hat{F}$ may vary in an arbitrary fashion.

It is always possible to calculate t_c and r_c for a given launch angle (i.e. turning point velocity or horizontal wavenumber). Even if r_c is a discontinuous function of angle it is still possible to plot $(t_c/r_c - 1/c_o)$ as a function of cycle distance r_c since the latter is also a function of angle. Thus we can always write τ_n as a function of r_c, say $\tau_n = n\,(t_c - r_c / c_o) = n\,G(r_c)$. However this alone (in combination with $r = n\times r_c$) does not ensure that τ_n is a separable function of range r. The only function G that allows separation is $G(r_c) = g\, r_c^{\,q}$ (where g is a proportionality constant) since $G(r_c) = G(r/n) = g\, r^{\,q}\times n^{-q}$. Thus to see fringes (in the complex Fourier transform) we *must* have

$$(t_c - r_c / c_o)\, r_c^{\,-q} = g(H, c(z)) = A_m = const \tag{15}$$

for the *m*th fringe, and so

$$\tau_{n,0,0} = n(t_c - r_c / c_o) = r_c^{\,q}\times n\, g = r^q \times n^{1-q} g \tag{16}$$

where q and g are to be determined and q is a constant. It is shown in the Appendix A, Sect. A.3 that by using this equation to evaluate $d(\log \tau_{n,0,0})/d(\log r_c)$ we can evaluate β directly. From Eq. (16) the exponent in Eq. (14) is then $i\omega r^q \times (n^{1-q} g)$ and for the jth fringe we need

$$\omega r^q = A_j = const \tag{17}$$

but then taking logs and differentiating we find behaviour exactly as in Eq. (1) with $\beta = -q$. The implication is that no other behaviour is possible.

3.4 Condition for a constant relative phase fringe

The relative phase condition depends on $(\tau_{n,\mu,\nu} - \tau_{m,\mu,\nu})$, and it is shown in Appendix A that $(\tau_{n,\mu,\nu} - \tau_{m,\mu,\nu}) = (n - m)(t_c - r_c K/\omega)$. Following the arguments of the previous section through but starting with $(t_c - r_c K/\omega)$ instead of $(t_c - r_c /c_o)$ we find that Eq. (15) becomes

$$(t_c - r_c K / \omega)\, r_c^{\,-q} = g(H, c(z)) = A_j = const \tag{18}$$

for the *j*th fringe, and so

$$\tau_{n,\mu,\nu} - \tau_{m,\mu,\nu} = (n-m)(t_c - r_c K/\omega) = r_c{}^q \times (n-m)\, g = r^q \times (n-m)^{1-q}\, g \qquad (19)$$

Again it is shown in Appendix A that this equation can be used to evaluate β' directly.

3.5 Source and receiver depths

From the earlier equations, notably Eq. (8), the source and receiver depths have an effect on the striations but it is weak except for the fact that they can limit the range of angles (or modes) available to interfere. As noted in Appendix A the source and receiver depths contribute small time offsets around the time $t_{n,0,0}$ that separate the four impulses in each group. These offsets have little effect on the interference fringes and the main pattern is still a function of range.

Writing Eq. (8) another way by combining the source and receiver delays

$$F(\omega, r) = 4\sum_n a_n \exp(i\omega\tau_{n,0,0}) \sin\left(\omega\int_0^{z_s} \sin\theta / c\, dz\right) \sin\left(\omega\int_0^{z_r} \sin\theta / c\, dz\right) \qquad (20)$$

the sine terms are essentially WKB modes that individually could form patterns of horizontal stripes on a plot of frequency vs. range, but collectively average out to a uniform background for the striations caused by $\tau_{n,0,0}$.

In isovelocity water keeping r and z_s constant but varying z_r we see fringes with

$$\omega z_r = A = \text{constant} \qquad (21)$$

but these are not as deeply modulated as the fringes in range.

4
Specific sound speed profiles

We can now evaluate t_c, r_c, $\tau_{n,0,0}$ for some given profiles, converting $\tau_{n,0,0}$ to a function of range. We can then evaluate β either through the relation between $\tau_{n,0,0}$ and r or by the following formulas derived in Appendix A. For absolute phase fringes:

$$\beta = \frac{1-\cos\theta}{(c_o t_c / r_c - 1)} = \frac{S_o - S_p}{S_g - S_o} \tag{22}$$

and for relative phase fringes:

$$\beta' = \frac{c_o r_c}{(c_o t_c / r_c - \cos\theta)} \Bigg/ \left(\omega \frac{dr_c}{dK}\right) = -\frac{\partial S_p}{\partial S_g} = \frac{\sin\theta}{\frac{\partial}{\partial\theta}\left(\frac{c_o t_c}{r_c}\right)} \tag{23}$$

The latter β' for relative phase fringes corresponds to that calculated by Chuprov, and several of the results below can be found in Chuprov (1982). A summary of the results of Section IV is given in Table 1. In all the following examples the ducts are assumed to be one-sided, even though the parabolic and cosh profiles could obviously be extended to two-sided, doubling their cycle distances and times.

Figures 3(a, b) show t_c, r_c and Fig. 4 shows $\log(t_c - r_c/c_o)$ vs. $\log r_c$ for each case. The straightness of the lines in Fig. 4 shows the goodness of fit to a line of constant β and one can also see the variability between cases.

Sound Speed Profile	$\beta = -\frac{S_p - S_o}{S_g - S_o} = \frac{1-\cos\theta}{(c_o t_c / r_c - 1)}$	$\beta' = -\frac{\partial S_p}{\partial S_g} = \sin\theta \Big/ \frac{\partial}{\partial\theta}\left(\frac{c_o t_c}{r_c}\right)$	Approx.
$c = c_o$	$\cos\theta$	$\cos^2\theta$ *	1
$c(z) = c_o(1 + a z)$	$\frac{-3\cos^2\theta}{1 - \frac{7}{10}\tan^2\theta - \frac{3}{40}\tan^4\theta\cdots}$	$\frac{-3}{1 + \frac{3}{5}\sin^2\theta + \frac{3}{7}\sin^4\theta\cdots}$	-3
$k^2 = k_o^{\ 2}(1 - a z)$	$\frac{-3}{2 - \sec\theta}$	$\frac{-3}{2 - \sec^2\theta}$ *	-3
$c = c_o \cosh az$	∞	∞	∞
$k^2 = k_o^{\ 2}(1 - a^2 z^2)$	$\frac{2}{\sec\theta - 1} \approx \frac{4}{\theta^2}$	$\frac{2}{\sec^2\theta - 1} = \frac{2}{\tan^2\theta}$ *	$\to +\infty$
$c^2 = c_o^{\ 2}(1 + a^2 z^2)$	$\frac{-8\cos^2\theta}{\tan^2\theta}\frac{(1 + O(\theta^2))}{(1 + O(\theta^2))}$	$\frac{-4\cos^2\theta}{\tan^2\theta}\frac{(1 + O(\theta^2))}{(1 + O(\theta^2))}$	$\to -\infty$
$k^2 = k_o^{\ 2}\left(1 - (a z)^p\right)$	$\frac{(3 - 2\nu)}{2\nu - (2 - \sec\theta)}$	$\frac{(3 - 2\nu)}{2\nu - (2 - \sec^2\theta)}$	$\frac{3 - 2\nu}{2\nu - 1}$
$c^2 = c_o^{\ 2}\left(1 + (a z)^p\right)$	$\frac{\cos^2\theta\left(1 + O(\tan^2\theta)\right)}{\frac{2\nu - 1}{3 - 2\nu} + O(\tan^2\theta)}$	$\frac{\cos^2\theta\left(1 + O(\tan^2\theta)\right)}{\frac{2\nu - 1}{3 - 2\nu} + O(\tan^2\theta)}$	$\frac{3 - 2\nu}{2\nu - 1}$

Table 1: The slope of interference fringes β calculated according to Eq.(22) compared with the standard waveguide invariant β' according to Eq. (23) and their approximate forms for various sound speed profiles. For the general profile shape $\nu = 1 - 1/p$ and $\frac{3 - 2\nu}{2\nu - 1} = \frac{p + 2}{p - 2}$. The asterisks indicate solutions already published by Chuprov (1982).

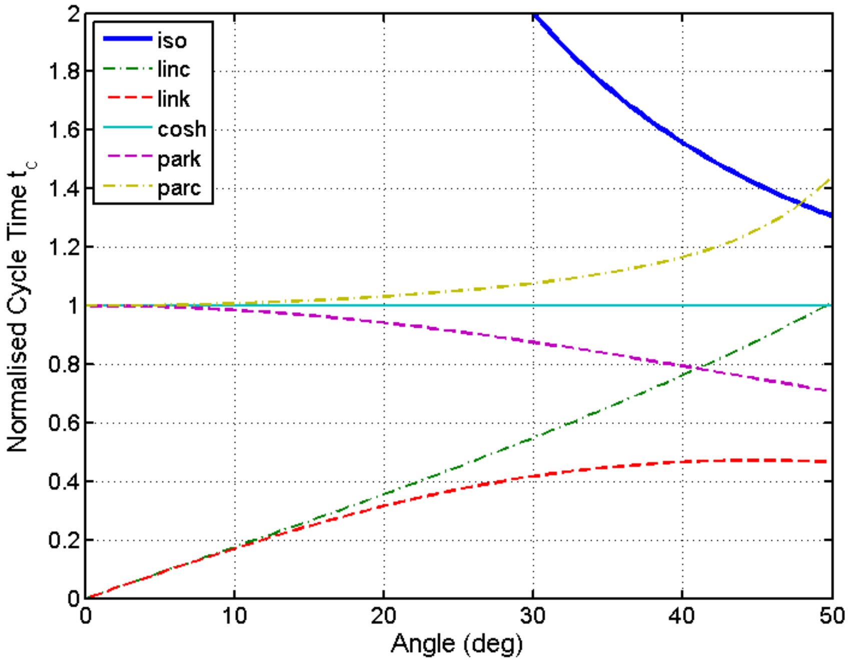

(a)

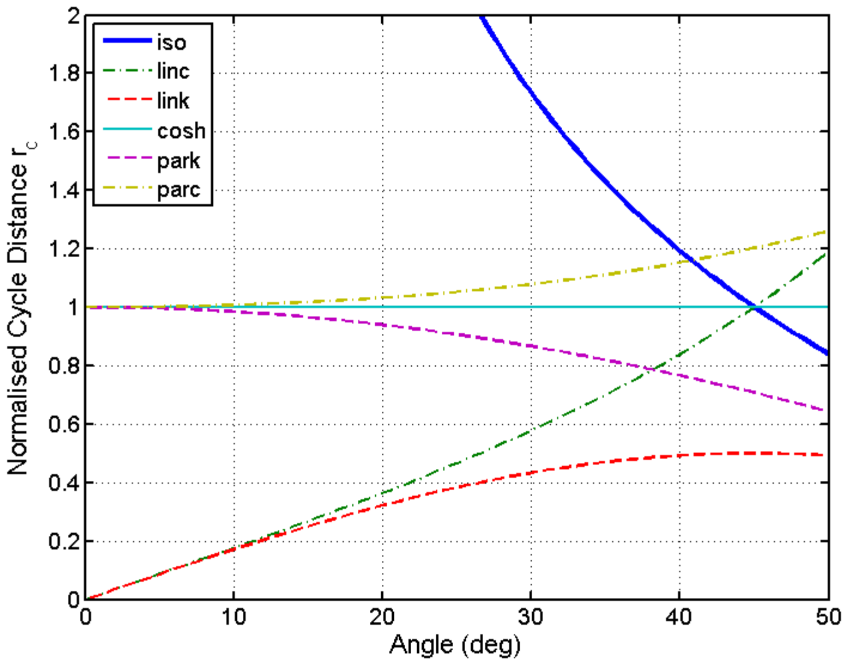

(b)

Figure 3: . (a) Cycle time vs. launch angle, (b) Cycle distance vs. launch angle, for six profiles as labelled: isovelocity; linear *c*; linear k^2; cosh; parabolic k^2; parabolic c^2.

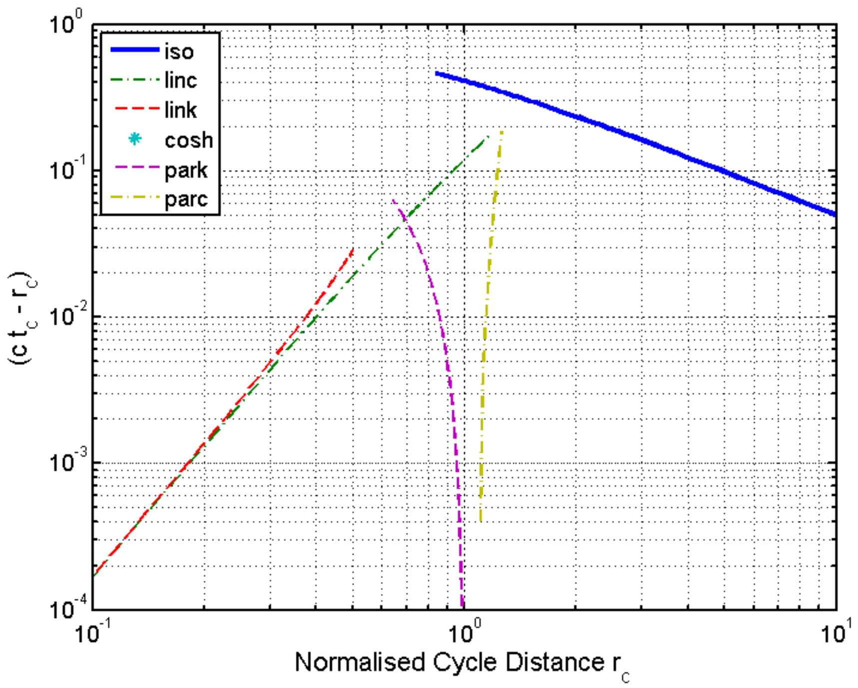

Figure 4: Corrected cycle time (t_c – r_c / c_o) vs. cycle distance r_c displayed on a loglog graph for the six profiles of Figs. 3. Gradients correspond to the respective β, so a straight line indicates that β is independent of launch angle.

4.1 Isovelocity

For an isovelocity profile the cycle time and distance are

$$t_c = 2H/(c\sin\theta) \tag{24}$$

$$r_c = 2H/\tan\theta \tag{25}$$

whose ratio is secθ, so both Eqs. (12) and (13) reduce to

$$\tau_{n,\mu,\nu}(r) = \frac{r}{c}\left(\sec\theta_{n,\mu,\nu} - 1\right) \tag{26}$$

as already found in Eq. (4). From Eqs. (22, 23)

$$\beta = \cos\theta \approx 1 \tag{27}$$

$$\beta' = \cos^2\theta \approx 1 \tag{28}$$

4.2 Uniform sound speed gradient

Assuming a uniform sound speed gradient with lower speed c_o

$$c(z) = c_o\,(1 + a\,z) \tag{29}$$

the cycle time and distance are

$$t_c = \frac{1}{a\,c_o}\log\left(\frac{1+\sin\theta_o}{1-\sin\theta_o}\right) = \frac{2}{a\,c_o}\operatorname{atanh}(\sin\theta_o) = \frac{2}{a\,c_o}\operatorname{asinh}(\tan\theta_o) \tag{30}$$

$$r_c = (2/a)\tan\theta_o \tag{31}$$

where θ_o is measured at the low sound speed boundary. Substituting Eqs. (30) and (31) into Eq. (13) with $c_L = c_o$ we find

$$\begin{aligned}\tau_{n,0,0}(r) &= \frac{r}{c_o}\left(\frac{\operatorname{asinh}(\tan\theta_o)}{\tan\theta_o} - 1\right) = -\frac{r}{c_o}\left(\tfrac{1}{6}\tan^2\theta_o - \tfrac{3}{40}\tan^4\theta_o + \cdots\right) \\ &\approx -r^3\,\frac{a^2}{24 c_o n^2}\end{aligned} \tag{32}$$

Note that the negative sign is because the chosen arbitrary datum was the slowest speed so that a time advance appears as negative delay. If instead we had substituted in the complete Eq. (12) there would have been an additional source and receiver term. The source term reduces, after some algebra, to

$$\mu\,r_s\left(\frac{t_s}{r_s} - \frac{t_c}{r_c}\right) = \mu\,r_s\left[\left(\frac{1}{c_s} - \frac{1}{c_o}\right) - \frac{a^2 c_o^{\,2}}{6}\left(\frac{r_s^{\,2}}{c_s^{\,3}} - \frac{r_c^{\,2}}{c_o^{\,3}}\right)\right] \tag{33}$$

is demonstrably small compared with the rest of Eq. (32). The value of β and β' [Eqs. (22) and (23)] are

$$\beta = \frac{-3\cos^2\theta}{1 - \tfrac{7}{10}\tan^2\theta - \tfrac{3}{40}\tan^4\theta} \approx -3 \tag{34}$$

$$\beta' = \frac{-3}{1 + \tfrac{3}{5}\sin^2\theta + \tfrac{3}{7}\sin^4\theta} \approx -3 \tag{35}$$

and both approximate to the familiar result. Figure 4 shows that the line whos gradient is β is indeed close to straight.

4.3 Linear k^2

The profile

$$k^2 = k_o^{\,2}\,(1 - a\,z) \tag{36}$$

i.e.

$$c^2 = c_o^{\,2}/(1 - a\,z) \tag{37}$$

is included here because it is often used in modal analysis. It can be shown that

$$t_c = \frac{4}{a c_o}(\sin\theta_o - \frac{2}{3}\sin^3\theta_o) \tag{38}$$

$$r_c = (4/a)\cos\theta_o \sin\theta_o \tag{39}$$

and

$$\tau_{n,0,0}(r) = \frac{r}{c_o}\left(\sec\theta_o - 1 - \tfrac{2}{3}\tan\theta_o \sin\theta_o\right) = -\frac{r}{c_o}\left(\frac{{\theta_o}^2}{6} + \cdots\right) \approx -r^3 \frac{a^2}{24 c_o n^2} \tag{40}$$

$$\beta = \frac{-3}{2 - \sec\theta} \approx -3 \tag{41}$$

$$\beta' = \frac{-3}{2 - \sec^2\theta} \approx -3 \tag{42}$$

which, to first order, is the same result as for linear $c(z)$.

4.4 The cosh profile

It is well known (see Eq. 5.45 of Tolstoy and Clay, 1987) that the profile

$$c = c_o \cosh az \tag{43}$$

leads to perfect focusing with

$$t_c = \frac{\pi}{a c_o} \tag{44}$$

and

$$r_c = \frac{\pi}{a} \tag{45}$$

Inserting these in Eq. (13) we find $\tau_{n,0,0} = 0$ (for all focuses). Thus the sums in Eq. (7) reduce to either no terms or a single term with the exponential term being unity, and so the Fourier transform is either flat in frequency or non-existent. According to Eqs. (22) and(23) both β and β' are infinite. This behaviour is shown by the vertical fringes in Fig. 5 calculated with ORCA calculated with ORCA (Westwood, et al., 1996).

Considering a ray trace up to some maximum launch angle (e.g. Fig. 5.7 of Tolstoy and

Clay, 1987) and picking a specific receiver depth we see that for ranges near a focus there are no eigenrays at all (unless the receiver happens to be at the focal depth), and for ranges in between there is only one eigenray. This is confirmed by the inset ray trace at the top of Fig. 5. In other words calculation of travel time differences or delays becomes meaningless in this case.

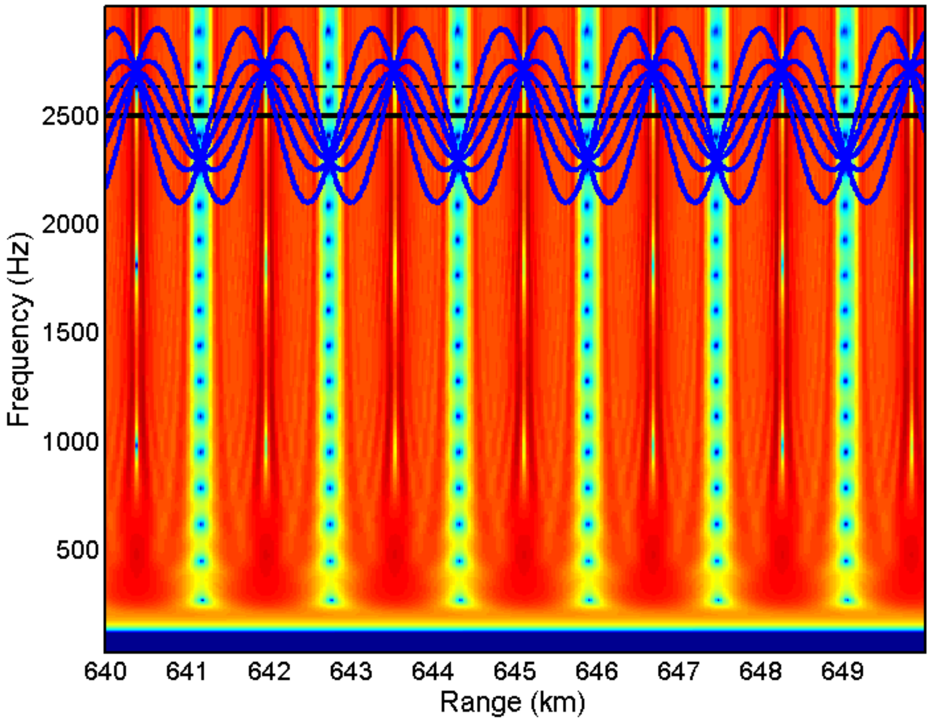

Figure 5: Striations calculated by ORCA for the (two-sided) cosh profile $c = c_o \cosh(az)$. The superimposed and aligned ray trace (receiver depth shown by dashed line) confirms that there may be no arrivals near the focus (when receiver depth is not equal to source complementary depth) and elsewhere only one eigenray, making an exactly repeating pattern each ray cycle.

4.5 Parabolic k^2 (over-curved)

The rather pathological behaviour for the cosh profile suggests that a slightly modified profile might be more interesting. The profile $c^2 = c_o{}^2(1 + a^2 z^2)$, though identical to cosh near $z = 0$, is slightly less tightly curved elsewhere whereas the profile

$$c^2 = c_o{}^2 / (1 - a^2 z^2) \tag{46}$$

is slightly more tightly curved. We take the latter, which can be written in terms of wavenumber $k(z)$ as

$$k^2 = k_o{}^2(1 - a^2 z^2) \tag{47}$$

The tighter curvature means that steep rays curve more than they would in the cosh case and therefore tend to focus at a shorter range. This is reflected in the cycle time and distance which can be shown to be

$$t_c = \frac{\pi}{a c_o}(1 + \cos^2 \theta_o)/2 \tag{48}$$

and

$$r_c = \frac{\pi}{a}\cos\theta_o \tag{49}$$

where θ_o is measured on the axis, $\cos\theta_o = \frac{c(z)}{c_T} = \frac{K}{k(z)}$, c_T is the turning point velocity, and K is the horizontal wavenumber. On substitution into Eq. (13) and defining the axial cycle distance as $r_{c0} = r_c(0)$ such that $r/n = r_c = r_{c0}\cos\theta_o$ we find

$$\begin{aligned} \tau_{n,0,0}(r) &= \frac{r}{c_o}\left(\frac{c_o t_c}{r_c} - 1\right) = \frac{r}{c_o}\frac{(1-\cos\theta_o)^2}{2\cos\theta_o} \\ &= \frac{(nr_{c0} - r)^2}{2c_o n r_{c0}} = \frac{n}{2c_o}\frac{(r_{c0} - r_c)^2}{r_{c0}} \end{aligned} \tag{50}$$

For each n only certain ranges can contribute impulses because of the limit on θ_o set by the maximum sound speed c_{max}. These ranges r are bounded by nr_{c0} and $nr_{c0}\cos\theta_{max}$.

$$n > r/r_{c0} > n\, c_o / c_{\max} \tag{51}$$

and at each range there are limits on n given by

$$n_{\min} = \frac{r}{r_{c0}};\ n_{\max} = \frac{r\, c_{\max}}{r_{c0}\, c_o}$$

Equations (22) and (23) give

$$\beta = \frac{2}{\sec\theta - 1} \approx \frac{4}{\theta^2} \to \infty \tag{52}$$

$$\beta' = \frac{2}{\sec^2\theta - 1} \approx \frac{2}{\tan^2\theta} \to \infty \tag{53}$$

which both tend to infinity in the small angle limit.

Although the formula (Eq. (50) is correct for this profile it is slightly misleading because, as we shall see in Sect. IV.G, a very slight change in the profile makes a dramatic change in the cycle distance formula, and this in turn completely alters the behaviour of Eq. (50). For now we note that whatever the fringe's shape they tail off towards range zero since β is large and positive.

4.6 Parabolic c² (under-curved)

An under-curved version of the cosh curve is

$$c^2 = c_o{}^2 (1 + a^2 z^2) \tag{54}$$

The cycle time and distance integrals are respectively elliptic integrals of the first and second kind. When evaluated at the lower limit (z = 0) these are both zero, and at the upper limit (the ray turning point) they both have their first argument equal to π/2 and so they are complete elliptic integrals of the first and second kind, and series formulas are given by Abramovitz and Stegun (1965) [Eqs. 17.3.11, 17.3.12].

$$t_c = \frac{2c_T}{a\,c_o{}^2} K(-\tan^2\theta_o) = \frac{\pi}{a\,c_o} \sec\theta_o \,(1 - \tfrac{1}{4}\tan^2\theta_o + \tfrac{9}{64}\tan^4\theta_o + \cdots) \tag{55}$$

and

$$r_c = \frac{2}{a} E(-\tan^2\theta_o) = \frac{\pi}{a} (1 + \tfrac{1}{4}\tan^2\theta_o - \tfrac{3}{64}\tan^4\theta_o + \cdots) \tag{56}$$

Again defining the axial cycle distance $r_{c0} = r_c(0) = \pi / a$ we find that now it is longer than for other ray angles. The resulting time separation is

$$\begin{aligned} \tau_{n,0,0}(r) &= \frac{r}{c_o} \frac{\left(\sec\theta_o - 1 - \tfrac{1}{4}\tan^2\theta_o\,(1+\sec\theta_o) + \tfrac{3}{64}\tan^4\theta_o\,(1 + 3\sec\theta_o)\right)}{(r_c / r_{c0})} \\ &\approx -\frac{r}{c_o} \frac{\tan^4\theta_o}{16(r_c / r_{c0})} \end{aligned} \tag{57}$$

But from Eq. (56)

$$\frac{\tan^2\theta_o}{4} \approx \frac{(r_c - r_{c0})}{r_{c0}} \tag{58}$$

so

$$\tau_{n,0,0}(r) \approx -\frac{r}{c_o (r_c / r_{c0})}\left(\frac{r_c - r_{c0}}{r_{c0}}\right)^2 = -\frac{(r - n\, r_{c0})^2}{c_o\, n\, r_{c0}} \tag{59}$$

where for each n only certain ranges can contribute impulses because of the limit on θ_o set by the maximum sound speed c_{max}. Thus at each range there are limits on n given by

$$n < r / r_{c0} < n\left(3 + (c_{\max} / c_o)^2\right)/ 4 \tag{60}$$

This is similar behaviour to the over-curved parabolic case but with fringes now tailing off on the far side of the foci. The values of β is

$$\beta = \frac{-8\cos^2\theta\left(1 + \tfrac{1}{4}\tan^2\theta - \tfrac{3}{64}\tan^4\theta \cdots\right)}{\tan^2\theta\left(1 - \tan^2\theta + \cdots\right)} \tag{61}$$

and β' is soluble but messy and can be seen as a special case of Eq. (83) (Sect. II.C.8) with $\nu = ½$.

$$\beta' = \frac{-4\cos^2\theta\left(1 + \tfrac{1}{2}\tan^2\theta - \tfrac{1}{32}\tan^4\theta \cdots\right)}{\tan^2\theta\left(1 - \tfrac{1}{2}\tan^2\theta + \cdots\right)} \tag{62}$$

4.7 General power law $k^2 = k_o^2\ (1 - (az)^p)$

The cycle time and distance integrals for the profile

$$k^2 = k_o^{\,2}\left(1 - (a\,z)^p\right) \tag{63}$$

(with $0 < p < \infty$ and $a\,z < 1$ for all z) can be written as

$$t_c = \left(\frac{4\,k_o^{\,2\nu-2}}{\omega\, pa}\right)\int_K^{k_o}\frac{k^3\,dk}{\sqrt{k^2 - K^2}\left(k_o^{\,2} - k^2\right)^{\nu}} \tag{64}$$

$$r_c = \left(\frac{4K\,k_o^{\,2\nu-2}}{pa}\right)\int_K^{k_o}\frac{k\,dk}{\sqrt{k^2 - K^2}\left(k_o^{\,2} - k^2\right)^{\nu}} \tag{65}$$

where

$$\nu = 1 - 1/p \tag{66}$$

and K is the horizontal wavenumber. The variety of profiles available is shown in Fig. 6, and the cycle time and distance behaviour is shown in Figs. 7(a, b).

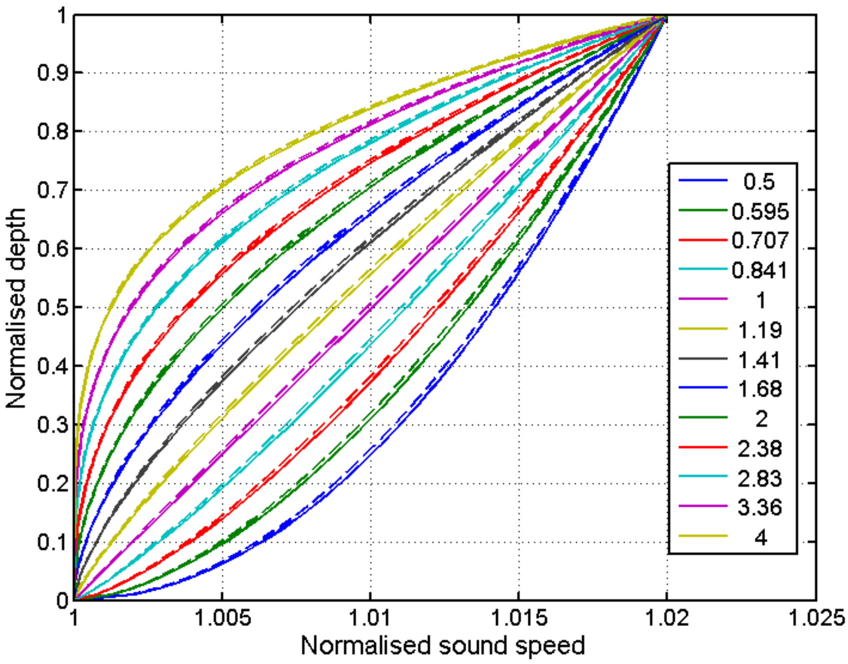

Figure 6: Normalised sound speed profiles $k^2 = k_o^{\,2}(1-(az)^p)$ for various values of the parameter *p* for which solutions (i.e. t_c, r_c, β) are available.

These can be solved in terms of the hypergeometric function ${}_2F_1(\alpha, \beta; \gamma, \zeta)$ with fixed values for α, β, γ. However, since the lower integral limit is always a ray turning point (where $k = K$) it vanishes, and the other limit is always ${}_2F_1(\alpha, \beta; \gamma, 1)$ which simplifies to the ratio of some gamma functions

$${}_2F_1(\alpha,\beta;\gamma,1) = \frac{\Gamma(\gamma)\Gamma(\gamma-\alpha-\beta)}{\Gamma(\gamma-\alpha)\Gamma(\gamma-\beta)} \tag{67}$$

the result is

$$t_c = \frac{2\sqrt{\pi}}{c_o a}\frac{\Gamma(2-\nu)}{\Gamma(3/2-\nu)}\sin^{1-2\nu}\theta_o\left(1-\frac{(2-2\nu)}{(3-2\nu)}\sin^2\theta_o\right) \tag{68}$$

$$r_c = \frac{2\sqrt{\pi}}{a}\frac{\Gamma(2-\nu)}{\Gamma(3/2-\nu)}\cos\theta_o\sin^{1-2\nu}\theta_o \tag{69}$$

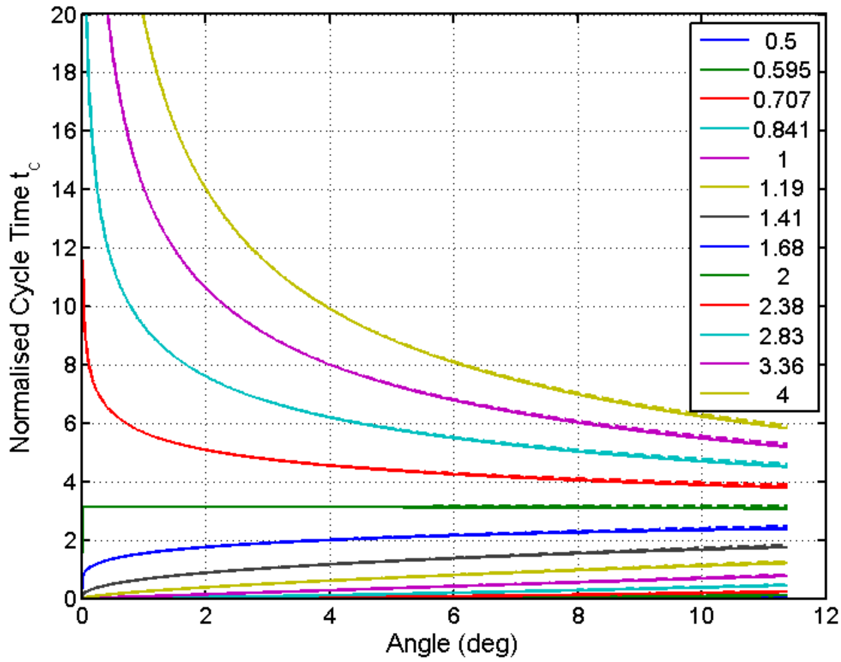

(a)

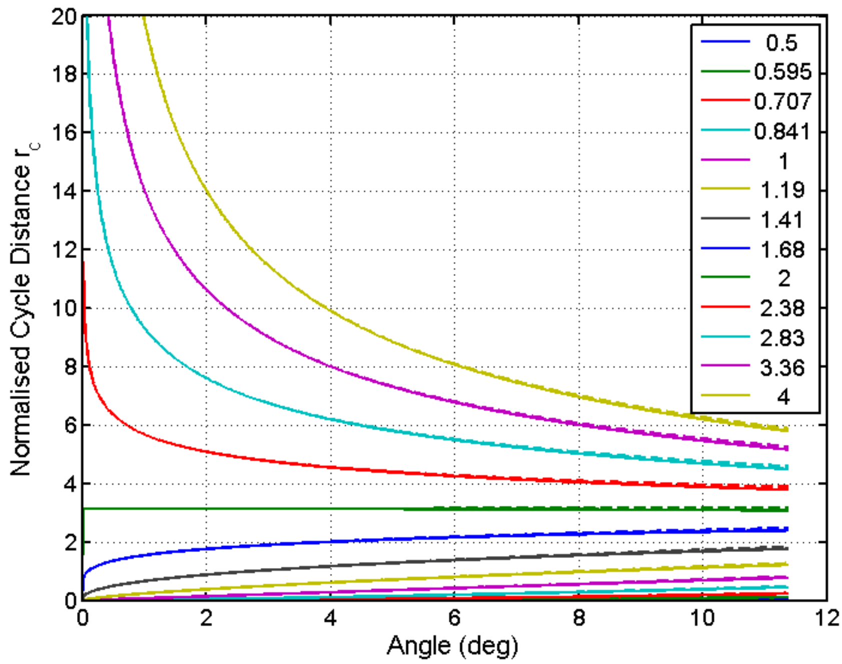

(b)

Figure 7: (a) Cycle time vs. launch angle, (b) Cycle distance vs. launch angle, for various values of the parameter p corresponding to the profiles in Fig. 6.

We can see that these reproduce some of the earlier results, namely linear and parabolic with p = 1, 2, (ν = 0, ½). In fact the behaviour of the isovelocity profile is also reproduced with $p = \infty$, (ν = 1) and $H = 1/a$. Figure 6(b) shows r_c vs. θ for a number of values of the parameter p. The time separation in terms of angle is

$$\begin{aligned}\tau_{n,0,0}(r) &= \frac{r}{c_o}\left(\frac{c_o t_c}{r_c} - 1\right) = \frac{r}{c_o}\left\{\sec\theta_o\left(1 - \frac{(2-2\nu)}{(3-2\nu)}\sin^2\theta_o\right) - 1\right\} \\ &\approx \frac{r}{c_o}\left\{\sin^2\theta_o \frac{(\nu - \frac{1}{2})}{(3-2\nu)} + \sin^4\theta_o \frac{(1+2\nu)}{8(3-2\nu)} + \cdots\right\}\end{aligned} \tag{70}$$

To write this in terms of r_c we need to substitute for θ_o. Provided ν is not too close to ½ the small angle approximation means that the cosine term in Eq. (69) can be ignored. At exactly ν = ½ we see why the solution for the parabolic profile [Eqs.(49, 50)] was "correct but misleading"; for $\nu <$ ½ the the power of the sine term is positive and so the cycle distance starts at zero for small angles whereas for $\nu >$ ½ the power is negative and the cycle distance starts at infinity. Only at exactly ν = ½ is it proportional to cosine. So mathematically we make the approximation

$$\sin\theta_o = \left(\frac{a\, r_c}{2\sqrt{\pi}} \frac{\Gamma(\frac{3}{2} - \nu)}{\Gamma(2-\nu)}\right)^{1/(1-2\nu)} \tag{71}$$

but graphically we can plot the logs of the exact Eq. (70) against the exact Eq. (69) as in Fig. 8. To first order the time separation is

$$\begin{aligned}\tau_{n,0,0}(r) &\approx \frac{n}{c_o} \frac{(\nu - \frac{1}{2})}{(3-2\nu)}\left(\frac{a}{2\sqrt{\pi}} \frac{\Gamma(\frac{3}{2} - \nu)}{\Gamma(2-\nu)}\right)^{2/(1-2\nu)} r_c^{(3-2\nu)/(1-2\nu)} \\ &\approx \frac{n^{-2/(1-2\nu)}}{c_o} \frac{(\nu - \frac{1}{2})}{(3-2\nu)}\left(\frac{a}{2\sqrt{\pi}} \frac{\Gamma(\frac{3}{2} - \nu)}{\Gamma(2-\nu)}\right)^{2/(1-2\nu)} r^{(3-2\nu)/(1-2\nu)}\end{aligned} \tag{72}$$

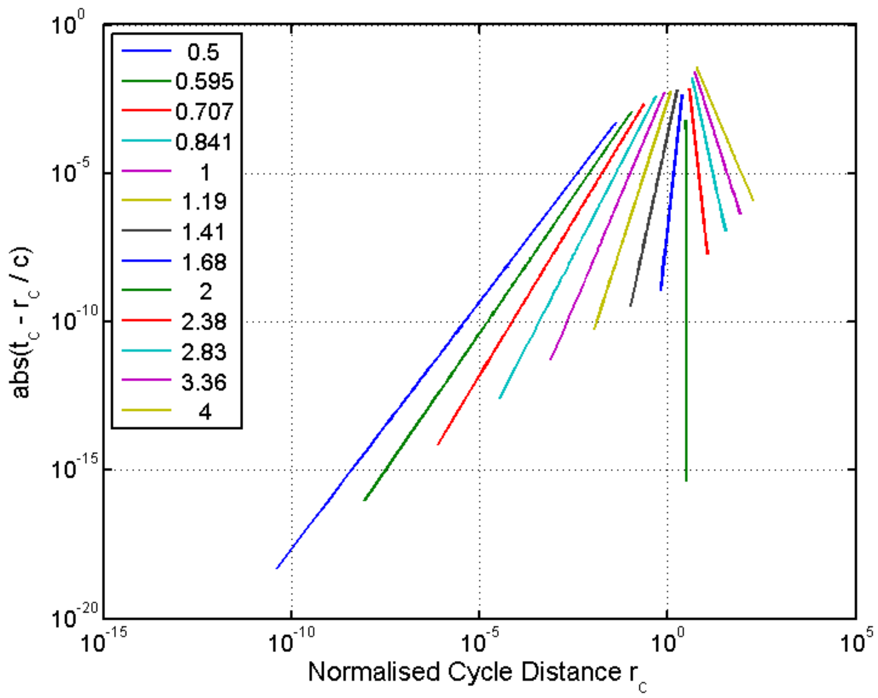

Figure 8: Corrected cycle time vs. cycle distance r_c displayed on a loglog graph for various values of the parameter p as shown in Figs. 6,7. Constant β corresponds to a straight line where $\beta = (p+2)/(p-2)$.

Inserting this into Eq. (14) and taking logs or directly from Eq.(22, 23) we find that

$$\beta = \left(\frac{3-2\nu}{2\nu-(2-\sec\theta)}\right) \approx \left(\frac{3-2\nu}{2\nu-1}\right) = \frac{p+2}{p-2} \tag{73}$$

$$\beta' = \left(\frac{3-2\nu}{2\nu-(2-\sec^2\theta)}\right) \approx \left(\frac{3-2\nu}{2\nu-1}\right) = \frac{p+2}{p-2} \tag{74}$$

The plot in Fig. 8 of the logs of the exact quantities in Eqs. (72) and (69) confirms that these formulas behave well even near $p = 2$. Thus it is possible to find β varying from 1 with large p (quasi-isovelocity) to infinity with $p = 2$ (parabolic), and from minus infinity, through –3 down to –1 with $p = 0$. For p slightly greater than 2, β is large and positive (sloping down towards range zero); for p slightly smaller than 2, β is large and negative (sloping down towards infinite range). Some examples of the striation patterns are shown in Fig. 9.

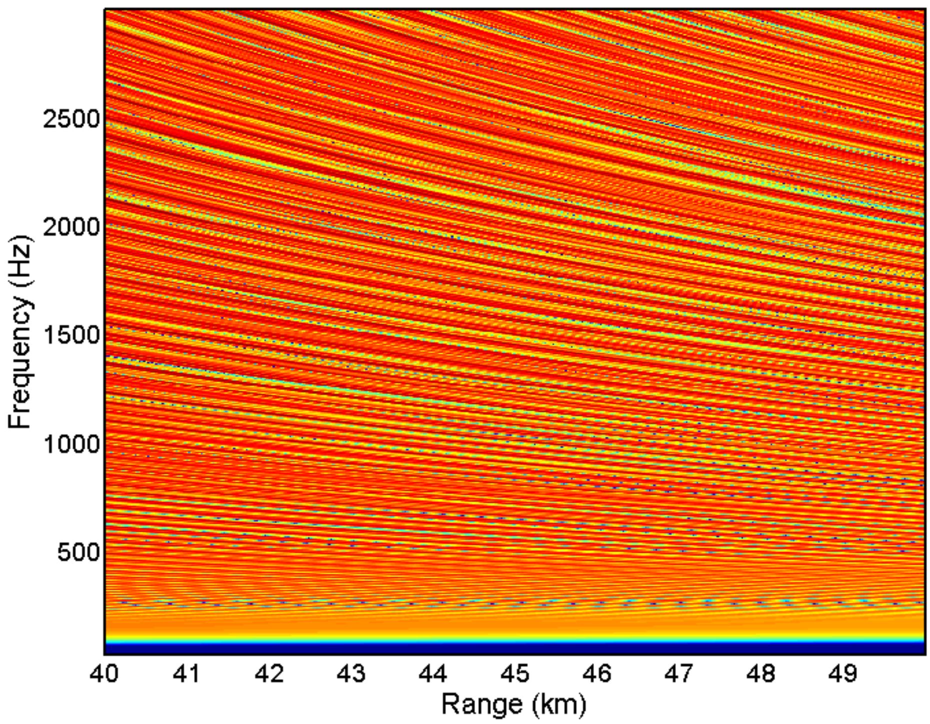
2500
2000
1500
1000
500
Frequency (Hz)
40
41
42
43
44
45
46
47
48
49
Range (km)

(a)

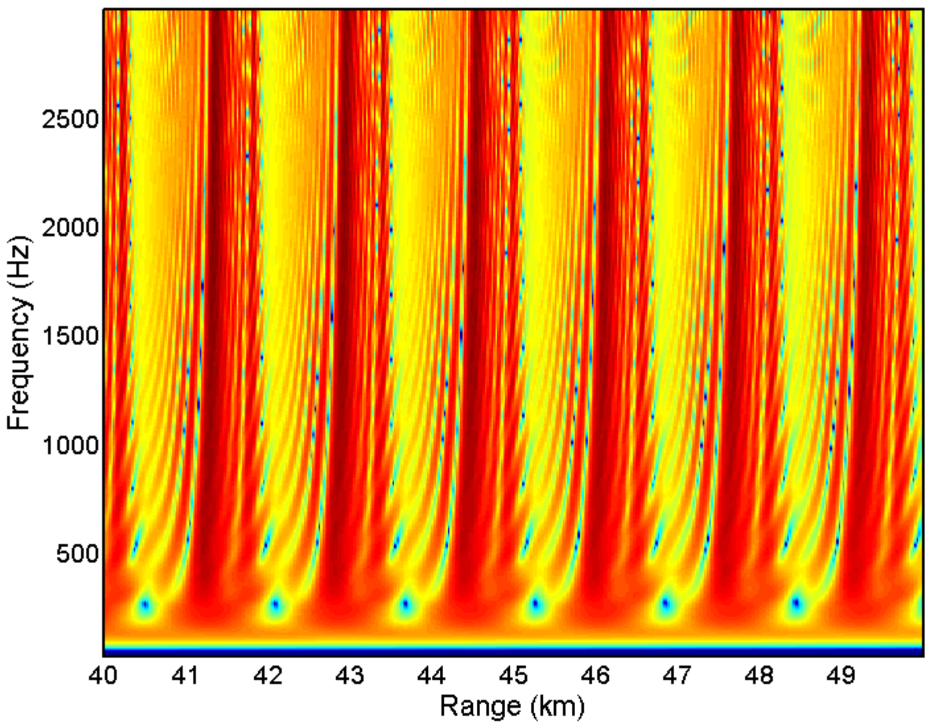
2500
2000
1500
1000
500
Frequency (Hz)
40
41
42
43
44
45
46
47
48
49
Range (km)

(b)

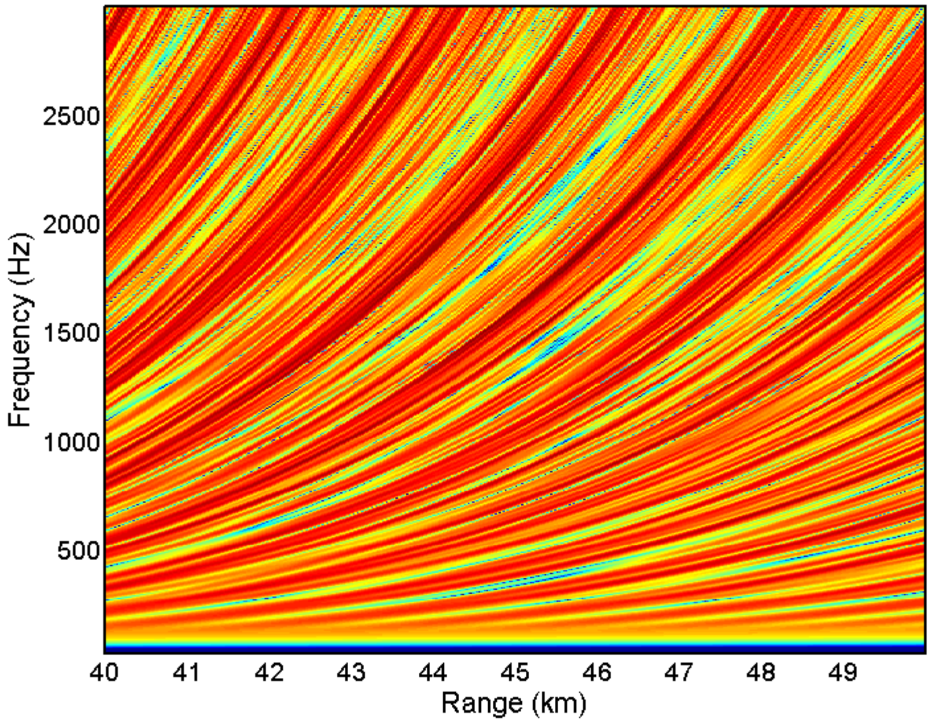

(c)

Figure 9: Striations calculated by ORCA for the power law $c^2 = c_o^2/(1-(az)^p)$ with (a) *p* =0.5, (b) *p* =2.0, (c) *p* =2.5. The fringes follow $\beta = (p+2)/(p-2)$ closely.

4.8 General power law $c^2 = c_o^2\,(1 + (az)^p)$

The solutions for the profile

$$c^2 = c_o^2\left(1+(a\,z)^p\right) \tag{75}$$

(with $0 < p < \infty$ and $a\,z < 1$ for all *z*) can also be written in terms of hypergeometric series. The cycle time and distance integrals can be written as

$$t_c = \left(\frac{4\,c_T c_o^{\,2\nu-2}}{pa}\right)\int_{c_o}^{c_T}\frac{dc}{\sqrt{c_T^{\,2}-c^2}\left(c^2-c_o^{\,2}\right)^{\nu}} \tag{76}$$

$$r_c = \left(\frac{4\,c_o^{\,2\nu-2}}{pa}\right)\int_{c_o}^{c_T}\frac{c^2\,dc}{\sqrt{c_T^{\,2}-c^2}\left(c^2-c_o^{\,2}\right)^{\nu}} \tag{77}$$

again with $\nu = 1 - 1/p$. Now

$$
\begin{aligned}
t_c &= \frac{2\sqrt{\pi}}{c_o a}\frac{\Gamma(2-\nu)}{\Gamma(3/2-\nu)}\sec\theta_o \tan^{1-2\nu}\theta_o \;{}_2F_1\left(1-\nu, 1/2; 3/2-\nu; -\tan^2\theta_o\right) \\
&= \frac{2\sqrt{\pi}}{c_o a}\frac{\Gamma(2-\nu)}{\Gamma(3/2-\nu)}\sec\theta_o \tan^{1-2\nu}\theta_o \\
&\quad\times\left(1 - \frac{(1-\nu)}{(3-2\nu)}\tan^2\theta_o + \frac{3(1-\nu)(2-\nu)}{2(3-2\nu)(5-2\nu)}\tan^4\theta_o + \cdots\right)
\end{aligned}
\tag{78}
$$

$$
\begin{aligned}
r_c &= \frac{2\sqrt{\pi}}{a}\frac{\Gamma(2-\nu)}{\Gamma(3/2-\nu)}\tan^{1-2\nu}\theta_o \left\{{}_2F_1\left(1-\nu, 1/2; 3/2-\nu; -\tan^2\theta_o\right)\right. \\
&\quad\left. + \frac{(1-\nu)}{(3/2-\nu)}\tan^2\theta_o \;{}_2F_1\left(2-\nu, 1/2; 5/2-\nu; -\tan^2\theta_o\right)\right\} \\
&= \frac{2\sqrt{\pi}}{a}\frac{\Gamma(2-\nu)}{\Gamma(3/2-\nu)}\tan^{1-2\nu}\theta_o \\
&\quad\times\left(1 + \frac{(1-\nu)}{(3-2\nu)}\tan^2\theta_o - \frac{(1-\nu)(2-\nu)}{2(3-2\nu)(5-2\nu)}\tan^4\theta_o + \cdots\right)
\end{aligned}
\tag{79}
$$

Again these formulas reproduce results for p = 1, 2, ∞, although the p = 1 case is not shown in this paper. Note that there is a sudden changeover from the power of the tangent being positive to negative at exactly $\nu = 1/2$ with a misleading parabolic solution (Eqs. (55, 56) in between [see Figs. 6(a, b)]. The time separation is

$$
\begin{aligned}
\tau_{n,0,0}(r) &= \frac{n}{c_o}\left(c_o t_c - r_c\right) \\
&= \frac{n}{c_o}\left\{\tan^2\theta_o \frac{(\nu - 1/2)}{(3-2\nu)} + O(\tan^4\theta_o)\right\}\frac{2\sqrt{\pi}}{a}\frac{\Gamma(2-\nu)}{\Gamma(3/2-\nu)}\tan^{1-2\nu}\theta_o
\end{aligned}
\tag{80}
$$

and we substitute the first order expression for r_c

$$
\tan\theta_o = \left(\frac{a\, r_c}{2\sqrt{\pi}}\frac{\Gamma(3/2-\nu)}{\Gamma(2-\nu)}\right)^{1/(1-2\nu)}
\tag{81}
$$

which, to first order, leads to the same expression as Eq. (72). Equations (22, 23) lead to

$$
\beta = \frac{\cos^2\theta\left(1 + At^2 - Bt^4 + Ct^6 + \cdots\right)}{(1-4A) + \left(8B - 1/2\right)t^2 + \left(-12C + B - 1/4 A + 3/8\right)t^4}
\tag{82}
$$

$$\beta' = \frac{\cos^2\theta G_2^{\ 2}}{G_1G_2 + (1+t^2)\left(-2A(G_1+G_2) + 4Bt^2(G_1+3G_2) - 6Ct^4(G_1+5G_2)\right)} \tag{83}$$

where

$$t = \tan\theta\,;\quad A = \frac{1-\nu}{3-2\nu}\,;\quad B = \frac{A}{2}\left(\frac{2-\nu}{5-2\nu}\right);\quad C = B\left(\frac{3-\nu}{7-2\nu}\right)$$

$$G_1 = 1 - At^2 + 3Bt^4 - 5Ct^6 + \cdots$$

$$G_2 = 1 + At^2 - Bt^4 + Ct^6 + \cdots$$

Again Eqs. (82, 83) both approximate to

$$\beta \approx \frac{1}{1-4A} = \left(\frac{3-2\nu}{2\nu-1}\right) = \frac{p+2}{p-2} \tag{84}$$

as long as $p \neq 2$.

5
Hybrids

5.1 Bilinear Duct

One can construct a sound channel from an upward and a downward linear k^2 duct as in Sect IV.C, for example, to make a bilinear duct (see e.g. Tolstoy and Clay, 1987). However the only effect in this context is that the values of t_c and r_c are doubled. Therefore after substituting in Eq. (13) there is no effect and we find again, $\beta = -3$.

5.2 Asymmetric Ducts

By the same reasoning as above one can construct $\tau_{n,0,0}$ for asymmetric ducts by adding the values of t_c or r_c for the upper and lower parts of the channel. As an example we take Eqs. (30) and (31) and insert them into Eq. (32), but now we assume the depth scale a in the upper part and b in the lower part. Note that the components of t_c and r_c are always positive

$$t_c = \frac{2}{|a| c_o} \operatorname{asinh}(\tan\theta_o) + \frac{2}{|b| c_o} \operatorname{asinh}(\tan\theta_o) \tag{85}$$

$$r_c = \frac{2}{|a|} \tan\theta_o + \frac{2}{|b|} \tan\theta_o \tag{86}$$

And, surprisingly, this makes absolutely no difference at all to $\tau_{n,0,0}$ and β since the a and b factor out in the ratio of t_c/r_c.

$$\tau_{n,0,0}(r) = \frac{r}{c_o}\left(\frac{\operatorname{asinh}(\tan\theta_o)}{\tan\theta_o} - 1\right) \approx -r^3 \frac{a^2}{24 c_o n^2} \tag{87}$$

and so beta is still –3.

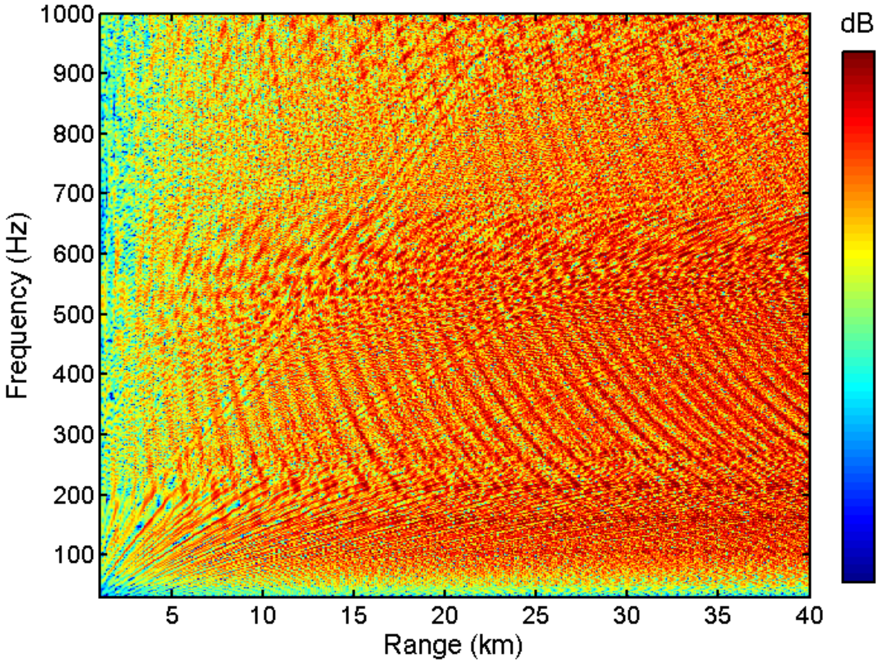

Figure 10: The transition from β = 1 at short range to β = –3 at long range in a range-independent upward refracting environment.

5.3 Combined refraction and reflection

Even with a fixed sound speed profile it is possible for the shape of the fringes to change because at different ranges different parts of the profile dominate. Figure 10 shows an example with upward refraction where at short range boundary-reflected paths dominate leading to $\beta = 1$, but at long range these die out leaving only refracted paths with $\beta = -3$.

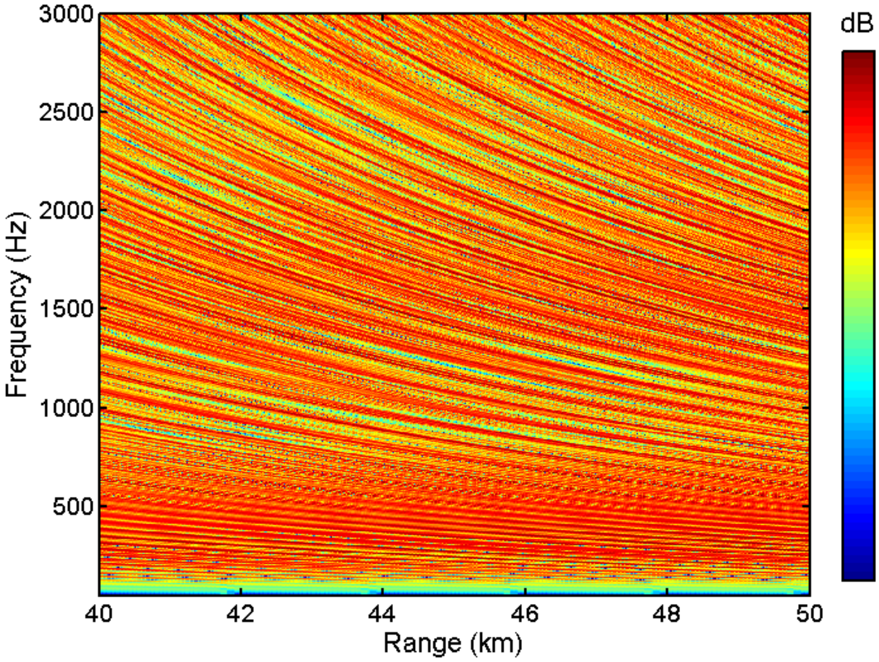

(a)

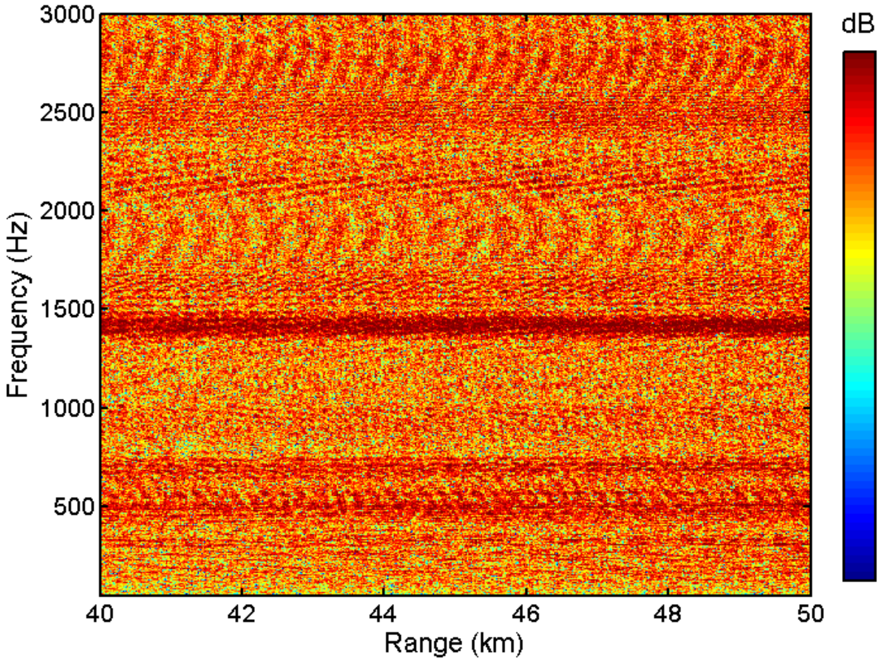

(b)

Figure 11: The effect on striations of adding randomness to the sound speed profiles in Fig.12. (a) pure linear profile and clear fringes; (b) 21 piece-wise linear layers resulting in smudged fringes.

5.4 Adding variability/randomness

One can take any of the analytical sound speed profiles considered above and numerically calculate the effects of adding some kind of randomness to the profile. From a ray tracing point of view sudden changes in sound speed or its first derivative will result in erratic behaviour of the cycle distance and time. From the previous analysis, therefore, one would expect the ensuing chaos to result in an absence of clear fringes. Figure 11 shows that this is indeed what happens. Figure 11(a) is the control result with no randomness; Fig.11(b) has rather slow variation (the profile is defined by only 21 points) which wipes out the fringes. The corresponding profiles are shown in Fig. 12.

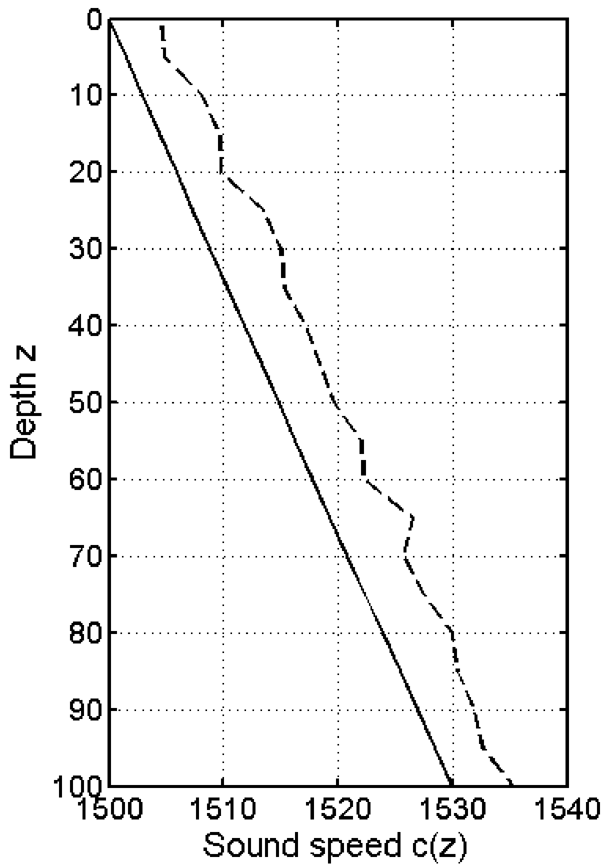

Figure 12: Sound speed profiles for Fig. 11, pure linear (solid); 21 piece-wise linear layers (dashed, offset by 5m/s).

6 Relationships, Invariance, and Range dependence

The previous sections investigated the conditions for fringes or striations to form and the dependence of the striation slopes (in frequency-range space) on sound speed profile. No previous theory was invoked and no assumptions were made other than the fringes having a Fourier transform relationship with the eigenray arrival times, i.e. the impulse response. Chuprov's (1985) original meaning of "invariance" was that the quantity β itself was independent of frequency, range, or source/receiver depth in a range-independent environment (Chuprov, 1985, p.94). All the formulas derived here, particularly Eqs. (73, 74), show this and demonstrate explicit dependence of β on the sound speed profile alone. A number of authors have considered range invariance too (D'Spain, 1999; Brown, et al., 2005). So far we have not commented on any range invariant properties since the environments in this paper were range-independent. Nevertheless the logical starting point that $\omega f(r)$ should be constant for some separable function of range f would still be a valid requirement for a fringe in a range-dependent environment.

To make the connection with range-dependence we use the general relationship derived in the Appendix (Eq. A2) between cycle time and cycle distance.

$$t_c - r_c\,K/\omega = (2/\omega)\int\sqrt{k^2 - K^2}\,dz = 2\int \sin\theta / c\,dz \qquad (88)$$

The extreme right hand side is exactly Weston's ray invariant (Weston, 1959) that describes the relation between ray angles and water depth as bathymetry or sound speed change with range. As written in the middle of the equation, the integral is exactly the WKB phase integral (Morse and Feshbach, 1953; pp1098-1099) which for a bound system, i.e. a reflecting or refracting duct evaluates to $(m + ½)\pi$, where m is the mode number. Thus in the adiabatic approximation the mode number itself is an invariant; individual modes do not lose energy to other modes and they stretch and shrink vertically to fit changes in sound speed and bathymetry as they propagate horizontally. Given that the right hand side is definitely an invariant (i.e. a constant for each m or initial ray angle) in a range-dependent environment, we deduce that the left hand side must also be invariant.

Comparing Eq. (88) with (19) we see that the eigenray time difference ($\tau_{n,\mu,\nu} - \tau_{m,\mu,\nu}$) which is equal to $(n-m)(t_c - r_c\,K/\omega)$ must also be invariant with range-dependent environments. However β' is the differential of this quantity with respect to r_c [see Eq. (A21)] and r_c is not an invariant, and neither is $r_c^2 / (dr_c / dK)$ so the outcome is that β' is not generally invariant. Comparing Eq. (16) with (19) we see that the absolute time $\tau_{n,0,0}$

is also not an invariant.

Nevertheless it is possible to see how the striations will be modified by a change in depth. Harrison and Siderius (2003) showed that the full field, and explicitly the multipath travel times in an (adiabatic) isovelocity range-dependent environment obey

$$t_{n,\mu,\nu} = r/c + \frac{\left(2n + \mu z_s / H_s + \nu z_r / H_r\right)^2}{2c\int_0^r dr / H^2} \tag{89}$$

Following the argument after Eq. (8) this means that fringes occur when

$$\frac{\omega}{\int_0^r dr / H^2} = A = \text{constant} \tag{90}$$

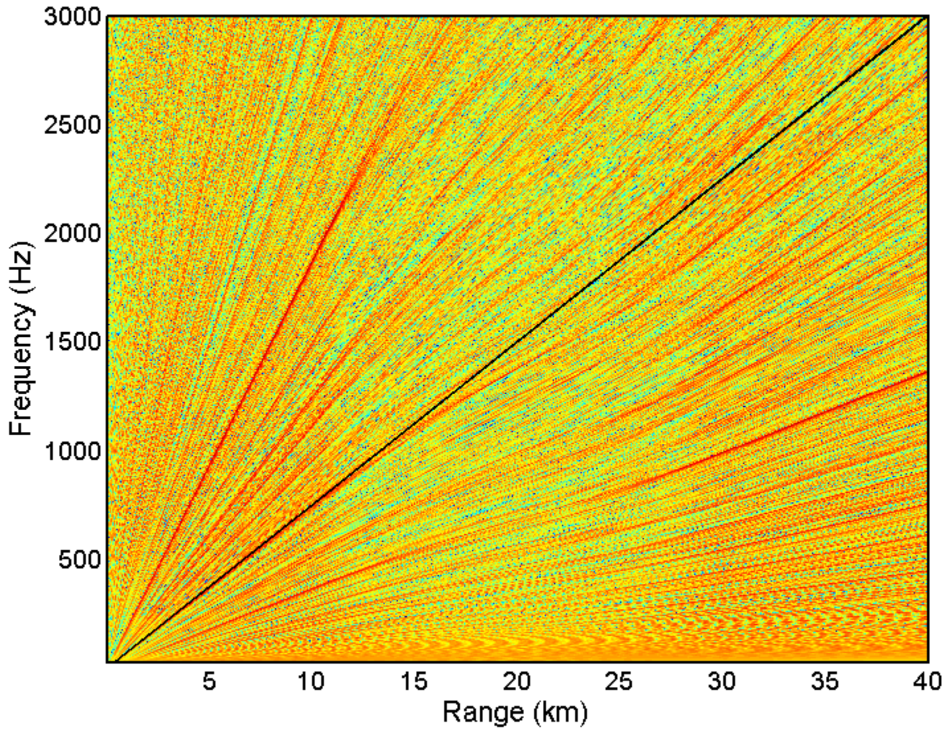

(a)

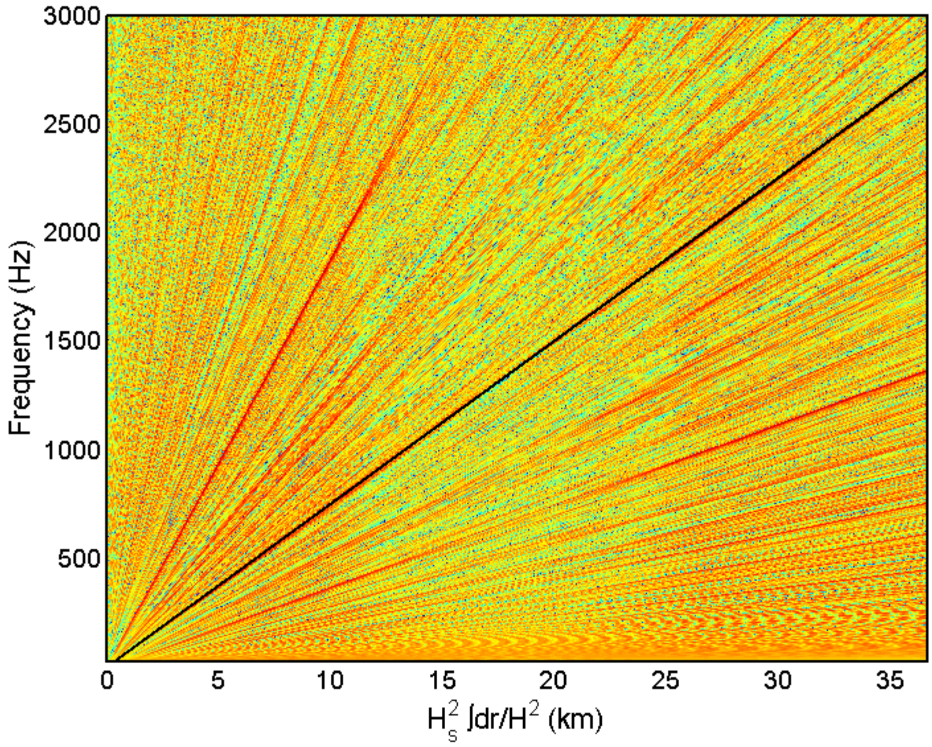

(b)

Figure 13: Striations with variable water depth. Piece-wise linear bathymetry defined by five equally spaced depths [100 100 120 100 100] m. Plot of frequency against (a) *r*, and (b) $H_s{}^2 \int_0^r dr / H^2$.

Thus the otherwise straight fringes (proportional to *r*) might be skewed by a dip in the seabed, for instance. Figure 13 shows this effect for piece-wise linear bathymetry with five depths of 100, 100, 120, 100, 100 m at 8km intervals. In Fig. 13(a) this distortion is shown in a plot of ω vs. *r*, and the fringes are clear on both sides of the dip. One could calculate the integral analytically in this case and superimpose a calculated fringe shape. Instead we choose to plot in Fig. 13(b) ω vs. $H_s{}^2 \int_0^r dr / H^2$ and thus demonstrate the proportionality of Eq. (90) through the straightness of the fringes. The effectiveness of this correction is indeed striking.

7
Some implications for reverberation

Reverberation as a function of travel time consists of echoes from scatterers at progressively greater range from source and receiver, so at first sight one would expect striations, being a propagation effect, to appear in the spectrum of broad band reverberation. Experimentally striations are occasionally seen in reverberation, but not always. Some possible reasons why are offered by this paper's approach.

- Source/receiver collocation: Horizontal separation of source and receiver will cause differences between outward and return propagation fringes which may blur reverberation striations, at least at short range.

- Smooth sound speed profile: To see striations the sound speed must be a reasonably smooth function of depth (e.g. continuous second derivative, avoiding real or false caustics) so that the time separation of the multipath impulses varies smoothly with angle (and therefore cycle distance).

- Number of eigenrays: At least a few eigenrays of comparable strength are required to make interference fringes. If either source, receiver, or scattering surface is near to the highest sound speed in the duct the number of eigenrays with refraction turning points will be small leaving only steep rays that interact with both boundaries to form fringes. There is also scope for differences between the outward and return paths.

8 Conclusions

Striation patterns in the propagation spectrum can be thought of as the result of range variation of the multipath impulse response, and so they can be calculated from travel times and therefore ray cycle times and cycle distances. The waveguide invariant β quantifies the range variation of these interference fringes and it has been determined for a number of sound speed profiles including the power law of depth $c^2(z) = c_o{}^2/(1-(az)^p)$ and $c^2(z) = c_o{}^2(1+(az)^p)$. It was shown that the cosh profile is a pathological case (which is close to a parabolic profile or $p = 2$ in the above formulas) which does not exhibit striation because the exact focusing results in only a single eigenray arrival for all ranges and depths and therefore no interference.

By considering absolute arrival times or time differences it was possible to derive a β for absolute phase and a β' for relative phase in each of the sound speed profile cases. Both can be written in terms of group and phase slownesses, and most of the relative phase formulas are well known.

The approach shows the clear dependence of the striations' β on path lengths rather than the corresponding eigenray amplitudes. For this reason addition of randomness to the sound speed profile leads to erratic behaviour of the cycle time and cycle distance with launch angle, and consequently striation patterns become blurred. Although the propagation spectrum and its interference patterns constitute part of the inputs for geoacoustic inversion, the value of β by itself is not directly related to seabed properties, even if the seabed is layered.

The distorting effect of variable bathymetry on the fringes was considered. In isovelocity water this distortion can be eliminated by plotting the fringes against frequency and $H_s{}^2\int_0^r dr'/H^2$ rather than r itself.

References

Abramovitz, M., and Stegun, I.A. (**1972**). *Handbook of Mathematical Functions*, Dover, NY.

Brekhovskikh, L.M. and Lysanov, Y.P. (1991). *Fundamentals of Ocean Acoustics*, 2nd ed. (Springer-Verlag, NY, 1991), pp.140-145.

Brown, M.G., Beron-Vera, F.J., Rypina, I., Udovydchenkov, I.A. (**2005**). "Rays, modes, wavefield structure, and wavefield stability", *Journal of the Acoustical Society of America*, **117**, 1607-1610.

Chuprov, S.D. (**1982**). "Interference structure of a sound field in a layered ocean", in *Ocean Acoustics, Current Status*, edited by L.M.Brekhovskikh and I.B. Andreyeva (Nauka, Moscow, 1982, pp. 71-91), and Washington DC: Joint Publications Research Service, 1985, pp. 88-111.

Cockrell, K.L., and Schmidt, H. (**2010**). "Robust passive range estimation using the waveguide invariant", *Journal of the Acoustical Society of America,* **127**, 2780-2789.

D'Spain, G.L. and Kuperman, W.A. (**1999**). "Application of waveguide invariants to analysis of spectrograms from shallow water environments that vary in range and azimuth", *Journal of the Acoustical Society of America*, **106**, 2454-2468.

Goldhahn, R., Hickman, G., and Krolik, J. (**2008**). "Waveguide invariant broadband target detection and reverberation estimation", *Journal of the Acoustical Society of America,* **124**, 2841-2851.

Harrison, C.H., and Siderius, M. (**2003**). "Effective parameters for matched field geoacoustic inversion in range-dependent environments", *IEEE Journal of Oceanic Engineering*, **28**, 432-445.

Harrison, C. H., and Nielsen, P. L. (**2007**). **"**Multipath pulse shapes in shallow water: Theory and Simulation", *Journal of the Acoustical Society of America*, **121**, 1362-1373.

Heaney, K.D. (**2004**). "Rapid geoacoustic characterization: applied to range-dependent environments", *IEEE Journal of Oceanic Engineering*, 43-50.

Hudson, R.F. (**1983**). "A horizontal range vs. depth solution of sound source position under general sound velocity conditions using the Lloyd's mirror interference pattern", Master's Thesis, Naval Postgraduate School, Monterey.

Kim, S., Kuperman, W.A., Hodgkiss, W.S., Song, H.C., Edelman, G.F., and Akal, T. (**2003**). "Robust time reversal focusing in the ocean", *Journal of the Acoustical Society of*

America, **114**, 145-157.

Morse, P.M., and Feshbach, H. (**1953**). “Methods of theoretical physics”, McGraw-Hill, NY.

Quijano, J.E., Zurk, L.M., and Rouseff, D. (**2008**). “Demonstration of the invariance principle for active sonar”, *Journal of the Acoustical Society of America*, 1329-1337.

Rouseff, D. (**2002**). “Statistics of the waveguide invariant distribution in a random ocean”, in *Impact of Littoral Environment Variability on Acoustic Predictions and Sonar Performance*, Eds. N.G. Pace and F.B. Jensen, Kluwer, 369-376.

Søstrand, K.A. (**2005**). “Range localization of 10-100 km explosions by means of an endfire array and a waveguide invariant”, *IEEE Journal of Oceanic Engineering*, **30**, 207-212.

Tolstoy, I. and Clay, C.S. (**1987**). “*Ocean Acoustics. Theory and experiment in underwater sound*”, Am. Inst. Phys.

Turgut, A., Orr, M., and Rouseff, D. (**2010**). “Broadband sourcelocalization using horizontal-beam acoustic intensity striations”, *Journal of the Acoustical Society of America*, **127**, 73-83.

Yang, T.C. (**2003**). “Beam intensity striations and applications”, *Journal of the Acoustical Society of America*, **113**, 1342-1352.

Weston, D.E. (**1959**). “Guided propagation in a slowly varying medium”, *Proceedings of the Physical Society London*, **73**, 365-384.

Annex A: Some useful relationships

A.1. Exact relationships: single eigenray

By considering an element of a ray of length *ds* at grazing angle θ the horizonal and vertical excursions *dr*, *dz*, and the time increment *dt* are related, for angular frequency ω and local wavenumber $k(z) = \omega / c(z)$, by

$$k\,ds = \omega\,dt = k\cos\theta\,dr + k\sin\theta\,dz \tag{A1}$$

Integrating in *z* from one side of the duct to the other ($z = 0,H$), or to a ray turning point, whichever is the sooner, invoking Snell's law, and multiplying by two we find a relation between cycle time t_c and cycle distance r_c

$$\omega t_c - K\,r_c = 2\int_0^H k\sin\theta\,dz = 2\int_0^H \sqrt{k^2 - K^2}\,dz \tag{A2}$$

Alternatively integrating from the same side down to the source or receiver depth $z_{s,r}$ we have

$$\omega t_{s,r} - K\,r_{s,r} = \int_0^{z_{s,r}} k\sin\theta\,dz = \int_0^{z_{s,r}} \sqrt{k^2 - K^2}\,dz \tag{A3}$$

or integrating over the depths of the unwrapped images

$$\omega t_n - K\,r = 2n\int_0^H \sqrt{k^2 - K^2}\,dz \pm \int_0^{z_s} \sqrt{k^2 - K^2}\,dz \pm \int_0^{z_r} \sqrt{k^2 - K^2}\,dz \tag{A4}$$

Differentiating Eq. (A2) with respect to *K* and noting that the differential of the right hand side is just $-\,r_c$ we find a relationship between the derivatives of t_c and r_c

$$\frac{d\,t_c}{d\,K} = \frac{K}{\omega}\frac{d\,r_c}{d\,K} \tag{A5}$$

and

$$\frac{d\,t_c}{d\,r_c} = \frac{K}{\omega} \tag{A6}$$

Similar relations hold for $t_{s,r}$ and $r_{s,r}$. The quantities t_c and r_c can be calculated through the following integrals across the water column (or at least between ray turning points)

$$t_c = \int 2/(c(z)\sin\theta)\,dz \tag{A7}$$

$$r_c = 2\int \cot\theta\,dz \tag{A8}$$

A.2. Approximate relationships: eigenray pair

The arrival time difference between the *m*th and *n*th eigenray ($t_{m,\mu,\nu} - t_{n,\mu,\nu}$) is estimated as follows, given that their angular separation is small. Cycle times and cycle distnces for *m*, *n* are labelled respectvely with a superscript "+", "–". Travel times are

$$t_{m,\mu,\nu} = t_s^{\,+} + m t_c^{\,+} + t_r^{\,+} \tag{A9}$$

$$t_{n,\mu,\nu} = t_s^{\,-} + n t_c^{\,-} + t_r^{\,-} \tag{A10}$$

Horizontal range is

$$r = r_s^{\,+} + m r_c^{\,+} + r_r^{\,+} \tag{A11}$$

$$r = r_s^{\,-} + n r_c^{\,-} + r_r^{\,-} \tag{A12}$$

Assuming that the difference between a "+" and a "–" quantity is accounted for by a slight change in angle $\delta\theta$ (i.e. $t_x^{\,+} = t_x^{\,-} + \delta\theta\, dt_x / d\theta$), we find, by subtracting Eqs. (A9, A10)

$$t_{m,\mu,\nu} - t_{n,\mu,\nu} = \delta\theta \frac{dt_s}{d\theta} + (m-n)\,t_c + m\delta\theta \frac{dt_c}{d\theta} + \delta\theta \frac{dt_r}{d\theta} \tag{A13}$$

Subtracting Eqs. (A11, A12) we have

$$0 = \delta\theta \frac{dr_s}{d\theta} + (m-n)\,r_c + m\delta\theta \frac{dr_c}{d\theta} + \delta\theta \frac{drt_r}{d\theta} \tag{A14}$$

Substituting for $\delta\theta$ we find

$$t_{m,\mu,\nu} - t_{n,\mu,\nu} = (m-n)\left(t_c + r_c \frac{\dfrac{dt_s}{d\theta} + m\dfrac{dt_c}{d\theta} + \dfrac{dt_r}{d\theta}}{\dfrac{dr_s}{d\theta} + m\dfrac{dr_c}{d\theta} + \dfrac{dr_r}{d\theta}} \right) \tag{A15}$$

and invoking Eq. (A4) this reduces to

$$t_{m,\mu,\nu} - t_{n,\mu,\nu} = (m-n)\left(t_c + r_c K/\omega \right) \tag{A16}$$

and by Eq. (A2) this is

$$t_{m,\mu,\nu} - t_{n,\mu,\nu} = (m-n)\left(t_c + r_c K/\omega\right) = 2(m-n)/\omega \int_0^H \sqrt{k^2 - K^2}\, dz \tag{A17}$$

Using the same method it is easy to show that, for instance

$$t_{n,+1,+1} - t_{n,+1,-1} = 2\left(t_r - r_r K/\omega\right) = 2/\omega \int_0^{z_r} \sqrt{k^2 - K^2}\, dz \tag{A18}$$

Comparing Eqs. (A17, A18) we see that the time separation of groups is always greater than separation of peaks within a group. For this reason the visible fringes, i.e. those with the closest spacing in frequency, tend to depend on the separation of the groups of four delta functions.

A.3 Formulas for beta

The quantity β is usually thought of as $d(\log\omega)/d(\log r)$. It was shown in Sect. III that for absolute phase fringes it can be expressed as

$$-\beta = \frac{\partial \log(\tau_{n,0,0})}{\partial \log(r_c)} = \frac{\partial \log(t_c - r_c/c_o)}{\partial \log(r_c)}$$

and for relative phase fringes it is

$$-\beta = \frac{\partial \log(t_{n+1,0,0} - t_{n,0,0})}{\partial \log(r_c)} = \frac{\partial \log(t_c - r_c K/\omega)}{\partial \log(r_c)}$$

Fringes of absolute phase:

$$-\beta = \frac{\partial \log(t_c - r_c/c_o)}{\partial \log(r_c)} = \frac{r_c}{(t_c - r_c/c_o)}\left(\frac{d\,t_c}{d\,r_c} - \frac{1}{c_o}\right) \tag{A19}$$

so, with no approximation, and making use of Eq. (A6) we have

$$\begin{aligned}\beta &= \frac{-r_c}{(t_c - r_c/c_o)}\left(\frac{K}{\omega} - \frac{1}{c_o}\right) = -\frac{K/\omega - 1/c_o}{(t_c/r_c - 1/c_o)} \\ &= \frac{1-\cos\theta}{(c_o t_c/r_c - 1)} = \frac{S_o - S_p}{S_g - S_o}\end{aligned} \tag{A20}$$

where S_g, S_p are group and phase slownesses $S_g = t_c/r_c$, $S_p = K/\omega$, and $S_o = 1/c_o$.

Relative phase fringes:

$$-\beta' = \frac{\partial \log(t_c - r_c\, K/\omega)}{\partial \log(r_c)} = \frac{-r_c^{\,2}}{(\omega t_c - r_c\, K)} \Bigg/ \frac{dr_c}{dK} \tag{A21}$$

but this can also be written in terms of slownesses using Eq. (A6) since

$$-\frac{\partial S_p}{\partial S_g} = -\frac{\partial (K/\omega)}{\partial (t_c / r_c)} = -\frac{r_c^{\,2}}{\omega(r_c\, dt_c/dK - t_c\, dr_c/dK)} = \frac{r_c^{\,2}}{(\omega t_c - r_c\, K)} \Bigg/ \frac{dr_c}{dK} \tag{A22}$$

so

$$\beta' = -\frac{\partial S_p}{\partial S_g} \tag{A23}$$

as stated by Chuprov [1982] and D'Spain and Kuperman [1999]. By substituting Eq. (A2) in the denominator of Eq. (A22) this can be reduced further to

$$\beta' = -\frac{r_c^{\,2}}{2\int_0^H \sqrt{k^2 - K^2}\, dz} \Bigg/ \frac{dr_c}{dK} \tag{A24}$$

as in Brown et al.(2005), Eq. (24), and differentiating r_c we have

$$\beta' = -\frac{r_c^{\,2}}{2\int_0^H \sqrt{k^2 - K^2}\, dz} \Bigg/ \int_0^H \frac{k^2 dz}{(k^2 - K^2)^{3/2}} \tag{A25}$$

Finally for modal propagation the right hand side of Eq. (A2) is twice the phase integral which is related to the mode number m so this can be written

$$\beta' = -\frac{r_c^{\,2}}{2\pi(m + ½)} \Bigg/ \int_0^H \frac{k^2 dz}{(k^2 - K_m^{\,2})^{3/2}} \tag{A26}$$

Document Data Sheet

Security Classification		Project No.
NATO UNCLASSIFIED		CASW
Document Serial No.	**Date of Issue**	**Total Pages**
NURC-FR-2011-001	February 2011	48 pp.

Author(s)

Harrison, C.

Title

The relation between the waveguide invariant, multipath impulse response, and ray cycles.

Abstract

The waveguide invariant, β, that manifests itself as interference fringes or "striations" in a plot of frequency vs source-receiver separation, is usually thought of as a modal phenomenon. This report shows that striations can be explained simply through the variation of the eigenray arrival times with range, in short, the variation of the multipath impulse response. It is possible to calculate β for a number of sound speed profiles analytically and to see what β depends on, why it switches from one value to another, how it depends on source-receiver depth, how it depends on variable bathymetry, and how smooth the sound speed profile needs to be for clear fringes. The analytical findings are confirmed by calculating striation patterns numerically starting from eigenray travel times in various stratified environments. Most importantly the approach throws some light on what can be deduced from β alone and the likelihood and utility of striations in reverberation.

Keywords

Waveguide invariant, interference fringe, striation, sound speed profile, closed-form solution, analytical solution, time domain.

Issuing Organization

NURC
Viale San Bartolomeo 400, 19126 La Spezia, Italy

[From N. America:
NURC
(New York) APO AE 09613-5000]

Tel: +39 0187 527 361
Fax:+39 0187 527 700

E-mail: library@nurc.nato.int

DISTRIBUTION LIST

NURC's Scientific Committee of National Representatives (SCNR) & National Liaison Officers

BELGIUM
DGMR SYS-N/M, Brussels
EGUERMIN, Oostende

CANADA
MOD CANADA
DRDKIM-2, Ottawa

DENMARK
MOD DENMARK
DANISH ACQUISITION AND LOGISTICS ORGANIZATION (DALO), Ballerup

ESTONIA
MOD ESTONIA

FRANCE
MOD FRANCE
O.N.E.R.A. (ISP), Chatillon

GERMANY
FIZBW - Bonn
FWG - BIBLIOTHEK, Kiel

GREECE
MOD GREECE
DEFENCE INDUSTRY & RESEARCH GENERAL DIRECTORATE, Holargos

ITALY
MOD ITALY
SEGREDIFESA - V° REPARTO, Roma

LATVIA
MOD LATVIA

NETHERLANDS
MOD NETHERLANDS
DEFENCE ACADEMY, Den Helder
ROYAL NETHERLANDS NAVY COMMAND, Den Helder

NORWAY
MOD NORWAY
NORWEGIAN DEFENCE RESEARCH ESTABLISHMENT - BIBLIOTEKET, Kjeller

POLAND
MOD POLAND
RESEARCH & DEVELOPMENT DEPARTMENT, Warsaw

PORTUGAL
MOD PORTUGAL
ESTADO MAIOR DA FORÇA AÉREA, Amadora

ROMANIA
MOD ROMANIA
ROMANIAN NATIONAL DISTRIBUTION CENTRE, Bucharest

SLOVENIA
MOD SLOVENIA

SPAIN
MOD SPAIN
SDG TECEN/DGAM, Madrid
INSTITUTO HIDROGRAFICO DE LA MARINA, Cadiz

TURKEY
MOD TURKEY
MILLI SAVUNMA BAKANLIĞI (MSB), Ankara
TURKISH NAVY RESEARCH CENTRE COMMAND, Istanbul

UNITED KINGDOM
DSTL KNOWLEDGE SERVICES, Salisbury

UNITED STATES
MOD USA
DEFENSE TECHNICAL INFORMATION CENTER (DTIC), Fort Belvoir, VA.